Astronomy
&
Astrophysics

High-resolution mapping of interstellar clouds with near-infrared scattered light[*]

M. Juvela[1], V.-M. Pelkonen[1], P. Padoan[2], and K. Mattila[1]

[1] Helsinki University Observatory, 00014, University of Helsinki, Finland
[2] Department of Physics, University of California, San Diego, CASS/UCSD 0424, 9500 Gilman Drive, La Jolla, CA 92093-0424, USA
    e-mail: ppadoan@ucsd.edu

ABSTRACT

Context. With current wide-field near-infrared (NIR) instruments the scattered light in the near-infrared can be mapped over large areas. Below $A_V \sim 10$ mag the surface brightness is directly proportional to the column density, and at slightly higher column densities the saturation of the intensity values can be corrected using the ratios of the intensity in different NIR bands. Therefore, NIR scattered light provides a promising new method for the mapping of quiescent interstellar clouds.

Aims. We develop a method to convert the observed near-infrared surface brightness into estimates of the column density. We study and quantify the effect that different error sources could have on the accuracy of such estimates. We also propose to reduce systematic errors by combining surface brightness data with extinction measurements derived from the near-infrared colour excess of background stars.

Methods. Our study is based on a set of three-dimensional magnetohydrodynamic turbulence simulations. Maps of near-infrared scattered light are obtained with radiative transfer calculations, and the maps are converted back into column density estimates using the proposed method. The results are compared with the true column densities. Extinction measurements are simulated using the same turbulence simulations, and are used as a complementary column density tracer.

Results. We find that NIR intensities can be converted into a reliable estimate of the column density in regions with A_V up to almost 20 mag. We show that the errors can be further reduced with detailed radiative transfer modelling and especially by using the lower resolution information available through the colour excess data.

Conclusions. We urge the observers to try this new method out in practice.

Key words. ISM: structure – ISM: clouds – infrared: ISM – ISM: dust, extinction – scattering – techniques: photometric

1. Introduction

The large scale distribution of the interstellar matter is affected by Galactic rotation, gravitational instabilities, and supernova explosions. Within the clouds the structure results largely from supersonic turbulence that is constantly fed by the large scaled phenomena and by stellar winds and outflows from newborn stars. At smaller scales the self-gravity becomes the dominant factor, keeping dense cloud cores together and eventually leading to core collapse and the formation of new stars. The magnetic fields are important at all scales. The flow of the matter is affected by a number of processes, each having its own imprint on the observed density distributions. Investigation of the cloud structure is important since it provides clues on the relative importance of turbulence, self-gravity and magnetic fields at different scales. It also provides information on different stages of the star-formation process and sets constraints on theories of star formation.

Information about the 3D spatial structure of interstellar clouds is obtained indirectly, through analysis of the observed radiation which represents an integral along the whole line of sight. Extended maps of interstellar clouds can be obtained with

several methods: (1) the integrated intensity of emission lines of various molecular or atomic tracers, especially CO and HI, (2) the thermal emission of dust grains at far-IR and sub-mm wavelengths, (3) star counts at optical or near-infrared wavelengths, (3) the near-infrared reddening of the light from background stars, (4) mid-infrared absorption toward dark clouds (Egan et al. 1998; Hennebelle et al. 2001), and (5) absorption toward bright X-ray background. Each of these methods has limitations, but gives a complementary view of the cloud structure.

A given molecular line is useful only in a limited density range, above the critical density of the transition, and below the optical depth where the line saturates. Molecular abundances depend on complicated, time-dependent chemical networks and, furthermore, depletion onto dust grains may cause additional effects. In the study of molecular lines, one should be able to estimate the excitation of the molecules and possible radiative transfer effects. Since the line-of-sight structure of the cloud is unknown, this cannot be done accurately. Abundances and excitation vary both on the plane of the sky and along each line of sight. It is well known that different molecules may peak at entirely different locations and, therefore, the estimated column density map depends critically on the selected tracer. Low extinctions around $A_V \sim 1$ pose a special problem because of the transition from atomic to molecular gas. Therefore, column density must be estimated by combining information from several

---

[*] Appendices are only available in electronic form at
http://www.edpsciences.org.

tracers with largely unknown abundances. The resolution obtained by single dish observations is usually some tens of arc seconds. Arc second resolution can be reached only with interferometric observations of small areas.

Thermal dust emission at far-IR and sub-mm wavelengths could provide a more straightforward picture of column density – if dust temperatures can be estimated and the dust to gas ratio remains constant. However, both dust temperature and FIR/sub-mm optical properties of dust grains may have significant spatial variations (Cambrésy et al. 2001; del Burgo et al. 2003; Dupac et al. 2003; Kramer et al. 2003; Stepnik et al. 2003; Lehtinen et al. 2004, 2006; Ridderstad et al. 2006). These may be due to grain growth by coagulation and ice mantle deposition (Ossenkopf & Henning 1994; Krugel & Siebenmorgen 1994) or physical changes in the grain material (e.g., Mennella et al. 1998; Boudet et al. 2005). Quiescent clouds have rather low intensity in the FIR/sub-mm and, because of the limited sensitivity, observations have concentrated on regions with $A_V \sim 10^m$ or above. For single dish observations the spatial resolution is typically worse than $\sim 10''$ in the sub-mm. FIR observations must be carried out with space borne instruments and, in spite of the shorter wavelengths, the resolution is not better.

Optical star counts are used to map the extinction mainly at low column densities (Wolf 1923) but can give reliable estimates up to $A_V \sim 5$ mag, depending on the available observations. High resolution is, however, hard to obtain since each resolution element must contain a large number of stars. In the optical region the stellar density drops rapidly above $A_V \sim 1$, but in the NIR the star counting method remains useful beyond $A_V \sim 20$, provided that deep K-band observations are available. However, in NIR the colour excess method yields better spatial resolution (e.g., Alves et al. 2001, 2002). The method is statistical in the sense that it relies on average properties of the background stars. Unlike star counting, the colour excess method provides an independent extinction estimate for each star, that is, for a number of very narrow beams through the cloud. The errors of these individual extinction estimates are dominated by the uncertainty on the (generally unknown) spectral type of the background star. An actual map of extinction is obtained by spatial averaging, and the reliability can be improved by combining results from more than two NIR bands (Lombardi & Alves 2001) and adaptive spatial resolution (Cambresy et al. 2002). With dedicated observations one can reach a resolution of $\sim 10''$. In the case of the commonly used 2MASS survey (limiting K_s magnitude ~ 15) the spatial resolution is, depending on the field location, a few arc minutes and the covered extinction range $A_V \sim 1$–15 mag.

The scattered light in dark clouds was first detected by photographic methods at optical wavelengths by Struve and Elvey (1936) and Struve (1936). They analyzed the light in terms of the dust scattering properties. Later on, Mattila (1970a,b) performed photoelectrical surface brightness observations of two dark nebulae and determined the dust albedo and scattering asymmetry parameter at the UBV bands. Haikala et al. (1995) made the first imaging of scattered light in a discrete diffuse/translucent cloud at the far UV wavelengths.

The first detection of NIR scattered light in a dark nebula illuminated by the normal interstellar radiation field (ISRF) was reported by Lehtinen and Mattila (1996). They also studied the relationship between J, H, and K band surface brightness vs. dust column density (measured by NIR colour excess method) which they found to be linear up to optical depth of ~ 1 in the wavelength band in question (their Fig. 8). From their Monte Carlo light scattering calculations they predicted that the linear relationship will saturate at optical depths of ~ 1.5 to 2

and then turn down. They also made the first determination of the albedo of Galactic interstellar grains in the JHK bands. The idea of using NIR surface brightness as a high-resolution probe of the dust density distribution in optically opaque clouds was presented by Lehtinen et al. in the ESO Press release 26a/2003[1] in connection with their VLT/ISAAC observations of DC303.8-14.2. Nakajima et al. (2003) presented JHK surface brightness images of the Lupus 3 dark cloud. They discussed their measurements in terms of scattered light from dust and presented diagrams of JHK surface brightness vs. A_V.

Padoan et al. (2006) proposed scattered near-infrared light as a direct measure of the cloud column density. That study was motivated by the images of the Perseus region obtained by Foster & Goodman (2006), which, in accordance with Lehtinen & Mattila (1996) and Nakajima et al. (2003), illustrated that large scale mapping of scattered intensity has become possible even for clouds illuminated by normal ISRF. In the near-infrared the dust properties are believed to be rather constant, resulting in smaller uncertainties in the scattering properties than at shorter wavelengths. In the normal extinction curve (Cardelli 1989) the optical depth in the K-band is about one tenth of the corresponding value in V-band. Therefore, in regions with A_V below 10 mag, the K-band intensity remains almost directly proportional to the dust column density. At higher extinctions the surface brightness starts to saturate, the effect being stronger at shorter wavelengths. Padoan et al. (2006) showed that if the saturation is taken into account, the combination of J-, H-, and K-bands can be used to estimate column densities for regions with A_V up to ~ 20 mag. The method avoids many shortcomings of the other methods listed above. Most importantly, it provides column density maps of interstellar clouds at a sub-arcsecond resolution. At low A the method is limited mainly by the sensitivity of the NIR observations.

In this paper we study in more detail the properties of column density estimates that are based on near-infrared scattering. We use the method presented by Padoan et al. (2006) as our starting point. We examine and quantify the effects of possible error sources, including differences in the cloud structure and column density, dust properties, and radiation field. We also address possible complications arising from near-infrared dust emission and diffuse background surface brightness. Furthermore, we propose to improve the reliability of the column density estimates with the help of colour excess measurements of background stars (the reddening data are a byproduct of the observations) and address the possibility of more detailed radiative transfer modelling.

In Sect. 2 we present the general method of converting NIR surface brightness into column density. In Sect. 3 we present the turbulence and the radiative transfer calculations used in our tests. The radiative transfer calculations provide simulated maps of near-infrared surface brightness that can be converted back to column density estimates using the proposed method. The results are compared with the true column densities of our model clouds in Sect. 4, where we will also examine the possibility of using colour excess data of the background stars to improve the accuracy of the column density estimates. In Sect. 5 we summarize our conclusions on the accuracy of the proposed method and discuss some particular sources of error. Direct radiative transfer modelling of observations is discussed in Appendix A and further discussion on some of the error sources is provided in Appendix B.
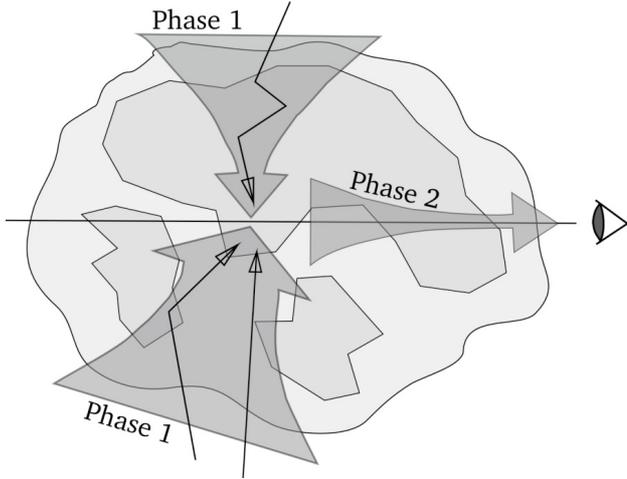
---

[1] http://www.eso.org/outreach/press-rel/pr-2003/phot-26-03.html

Fig. 1. A schematic view of the creation of the observed surface brightness of scattered light (see text). The figure shows an inhomogeneous cloud with arrows indicating the flow of photons. In the first phase external radiation is transported onto a selected line of sight where it is scattered toward the observer. Photons reach this line possibly after several scatterings and preferably through regions of low density. In the second phase radiation propagates out from the cloud along the selected sightline.

2. Conversion of near-infrared surface brightness to column density

Padoan et al. (2006) presented a method for transforming observations of near-infrared surface brightness into estimates of column density. The main points are repeated below. We assume that the cloud is illuminated by an isotropic radiation field, the observed intensity can be attributed to scattering from dust particles, and observations of a few near-infrared bands are available. Because scattering traces only the dust column density, a constant dust to gas ratio is assumed when results are transformed into total gas column density. The accuracy of these assumptions is discussed later in this paper.

In the optically thin case the intensity of the scattered light is directly proportional to the column density. When the optical depth becomes close to one, the surface brightness starts to saturate. In the schematic view of Fig. 1 we divide the scattering process into two phases. In the first phase the external radiation enters the cloud and is transported onto the selected sightline where it finally scatters toward the observer. In the second phase the radiation is propagated along the selected sightline toward the observer. During this phase the intensity is decreased by both absorption and scattering. This schematic view is useful to understand the reason why our method is based on a formalism (e.g. Eq. (1)) that corresponds to the radiation transfer along an individual line of sight, hence accounts only for the second phase. The reason is that the second phase is more important than the first for the relation between the surface intensity and the column density, as the first phase cannot generate strong radiation field variations within the cloud tightly correlated with the line-of-sight column density.

Because the incoming radiation field is attenuated during the first phase in a way that depends on the density structure of the cloud, different locations in the cloud could experience different radiation field intensities and this could affect the relation between the observed intensity and the dust column density, but this effect is relatively small for two reasons. First, a volume element is illuminated from all directions. In an inhomogeneous cloud the radiation propagates more freely through low density regions so that inside the cloud the field can be much stronger than what would be expected based on the mean optical depth. Second, photons can reach a given line of sight also after some scatterings. Most scatterings are in the forward direction so the radiation can again better reach deeper cloud regions. Both effects make the field strength resulting from the first phase relatively uniform within the cloud. During the second phase, instead, the attenuation depends on the optical depth (column density) of a particular line of sight and every absorption and scattering event decreases the observed intensity.

In the near-infrared the albedo of dust grains is close to one half (Lehtinen & Mattila 1996), so the scattering is a significant component of the total extinction. Taking into account the cloud inhomogeneity, the effect of the attenuation during the first phase is perhaps half of the effect during the second phase and, therefore, gives a smaller contribution to the relation between surface brightness and line-of-sight column density. The uncertainty in our method due to this small contribution from the first phase is studied with radiative transfer simulations.

The relation between surface brightness and column density follows from the solution of the radiative transfer problem. As explained above, the observed intensity is determined mainly by radiative transfer effects during the second phase. This suggests that a radiative transfer equation written for an individual line of sight should provide a good functional form for the solution. In the case of a homogeneous medium this results in the equation

$$I_\nu = a\,(1 - \mathrm{e}^{-bN}), \tag{1}$$

which gives the surface brightness of scattered light, I_ν, as a function of column density, N. In this formula, a and b are constants related to the dust properties and to the incoming radiation field. The constant b is clearly similar to an absorption coefficient. This analytical formula was already found to fit the simulation results of Padoan et al. (2006). We will examine these correlations for a larger set of cloud models in Sect. 4.1. In the limit of low optical depth Eq. (1) gives

$$I = a\,b\,N, \tag{2}$$

the intensity is directly proportional to the column density, and the product $a \times b$ describes the scattering that takes place per unit column density. If b is assumed to describe dust properties, the constant a would mostly reflect the intensity of the incoming radiation. However, the interpretation of these constants is not this straightforward. In the term $\exp(-b\,N)$, the constant b has the role of an extinction coefficient, while in Eq. (2) it would be a scattering coefficient. In the following we treat a and b simply as empirical parameters. We expect that if either the dust properties or the radiation field were changed, the values of both a and b would change.

At large optical depths one must correct for the non-linearity, i.e., the saturation of the surface brightness. Equation (1), written for each band separately, defines a parametric curve in the (I_J, I_H, I_K)-space. Each observed (I_J, I_H, I_K)-triplet should correspond to a point on this curve, and the parameter value N could be calculated if the constants a and b were known. We emphasize that Eq. (1) simply defines an empirical curve representing the observations. It gives a good description of the relation between surface brightness and column density, but is not necessarily the optimal function.

When no independent column density estimates are available, surface brightness observations can only be used to determine the ratios between the NIR bands. For example, by writing

Eq. (1) for the H and K bands, N can be eliminated and the H band can be expressed as a function of the K band,

$$I_H = a_H \times \left(1 - \left(1 - \frac{I_K}{a_K}\right)^{\frac{b_H}{b_K}}\right). \qquad (3)$$

The constants a_J, a_H, and a_K and the ratios b_J/b_K and b_H/b_K can be determined by fitting this curve to the observations. However, determination of the individual b constants requires additional information.

We have explained above that the b constants depend mainly on the properties of the dust grains. In the NIR, dust properties vary only relatively little. If the b constants are similar in different clouds, one can use values already established from observations of other similar objects. The a constants depend mainly on the radiation field that illuminates the cloud. The uncertainty of the intensity is often large, ~50%. This affects mostly the absolute scaling of the column density map. The spectral shape of the incoming radiation can also vary depending, for example, on the presence of nearby OB associations. However, if the relative values of the scattering cross sections are known, the spectrum can be estimated using observations of low extinction sightlines.

The expected values of the constants a and b can be determined by radiative transfer modelling, while the observed ratios of Eq. (3) can be used to correct the values of a and the ratios between the b constants. If a correction is necessary, either the radiation field or the NIR dust properties differ from their initially assumed values. Cloud properties, the average column density and the inhomogeneity, are also expected to have some effect. These will be studied in Sect. 3.

There is still another, more straightforward way to check the validity of Eq. (1). When NIR scattering is measured, the observations contain colour excess data for a large number of background stars. The resolution of the extinction map may be one or two orders of magnitude worse than the resolution of the surface brightness maps. However, it is sufficient to check the parameters of the surface brightness method and even to determine the values of the individual b constants. It is not clear whether the colour excess method is intrinsically more accurate. However, since the error sources and error properties of the two methods are very different, a comparison should be useful to test for systematic effects and to provide error estimates for the derived column density maps.

Once the constants are determined, Eq. (1) can be used to convert surface brightness values into column density. The conversion could be done for each band separately, by inverting Eq. (1),

$$N = -\frac{1}{b} \log\left(1 - I_\nu/a\right), \qquad (4)$$

In principle, observations at one wavelength would be sufficient. However, the use of several bands is more secure, and it brings additional information that can be used in the analysis (see, e.g., Appendix A). In this paper we assume that observations exist of J-, H-, and K-bands. Because of the noise in the observations and possible model errors the observed intensities do not fall exactly on the curve given by Eq. (1). For each map position, we find on this curve a point that minimizes a least square distance from the observed (I_J, I_H, I_K)-triplet. The corresponding column density is then obtained from Eq. (4).

3. Modelling of NIR scattering

In this section we describe the numerical modelling used to study the relation between the NIR surface brightness and the column density. The results are based on three-dimensional magnetohydrodynamic (MHD) turbulence simulations and Monte Carlo radiative transfer calculations.

3.1. MHD turbulence simulations

The density structure of our model clouds is based on six MHD turbulence simulations that provide a good approximation of the structure of interstellar clouds.

The first three model clouds – A, B, and C – have a resolution of 128^3 computational cells. In these models the turbulence is highly supersonic, with sonic rms mach numbers $M_s \sim 10$. The initial density and magnetic fields are uniform, and an external random force is applied to drive the turbulence at a roughly constant rms Mach number. In model C self-gravity is also included. Model A has approximate equipartition of magnetic and kinetic energy, the Alfvénic Mach number being $M_A \sim 1$. The models B and C have weaker magnetic fields and the turbulence is strongly super-Alfvénic with $M_A \sim 10$. These MHD simulations are the same used in Juvela et al. (2001) for estimation of molecular line cooling in inhomogeneous clouds, and the reader is referred to that article for further details.

The other three model clouds – D, E, and F – are from MHD simulations on grids of 250^3 computational cells, but the models are downsized to 125^3 cells for the radiative transfer calculations. The rms sonic Mach numbers are 0.6, 2.5, and 10.0, for D, E, and F, respectively. The initial density and magnetic field are uniform and the gas is assumed to be isothermal. The initial Alfvénic Mach numbers are $M_A \sim 10$. The volume-averaged magnetic field strength is constant in time because of the imposed flux conservation. The magnetic energy is instead amplified. The initial value of the ratio of average magnetic and dynamic pressures is $\langle P_m \rangle_{in}/\langle P_d \rangle_{in} = 0.005$, so the run is initially super-Alfvénic. The value of the same ratio at later times is larger, due to the magnetic energy amplification, but still significantly lower than unity, $\langle P_m \rangle_{in}/\langle P_d \rangle_{in} = 0.12$. The turbulence is therefore super-Alfvénic at all times. Turbulence is again set up as an initial large-scale random and solenoidal velocity field and is maintained with an external large-scale random and solenoidal force. Experiments are run for approximately 10 dynamical times in order to achieve a statistically relaxed state. The models D–E were used, for example, in Juvela et al. (2003) for estimation of [CII] cooling of inhomogeneous translucent clouds. Column density maps from models A, C, D, and E are shown in Fig. 2.

Supersonic and super-Alfvénic turbulence of an isothermal gas generates a density distribution with a very strong contrast of several orders of magnitude. It has been shown to provide a good description of the dynamics of molecular clouds and of their highly fragmented nature (e.g., Padoan et al. 1999, 2001, 2004). The most important property affecting the radiative transfer calculations is the degree of inhomogeneity. In this respect the models provide a wide range of conditions. Details about the numerical method used in the MHD simulations are given in Padoan & Nordlund (1999). All simulations use periodic boundary conditions, the effect of which is examined later in Sect. 4.1.
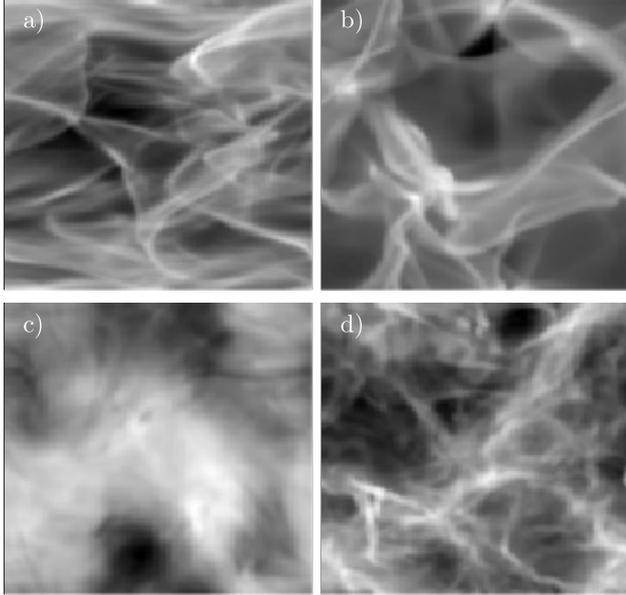
Fig. 2. Examples of the structure seen in the model clouds. The frames *a − d* show column density maps of models A, C, D, and E, respectively. The colour scales are logarithmic and independent for each frame.

Fig. 3. Histograms of A_V values in the six model clouds with average visual extinction $\langle A_V \rangle = 1.6$ mag. For model C the distributions are plotted for three orthogonal directions of observations. For the other models distributions are shown only for one direction.

3.2. Radiative transfer calculations

The flux of scattered radiation is calculated with a Monte Carlo program (Juvela & Padoan 2003; Juvela 2005), where sampling of scattered radiation is further improved with the "peel-off" method (Yusef et al. 1994). During each run, photons are simulated at one wavelength, and the scattered intensity, including multiple scatterings, is registered toward a selected direction. The result is an intensity map where the pixel size corresponds to the cell size of the model cloud. The maps size is therefore either 125 × 125 or 128 × 128 pixels. Maps are calculated for the three NIR bands *J*, *H*, and *K* (1.25, 1.65, and 2.2 μm), for three directions perpendicular to the faces of the cubic model cloud (directions *X*, *Y*, and *Z*) and for two diagonal directions (*D*1 and *D*2). The final maps are averages of several independent runs, allowing us to control the level of the numerical errors. In the following the uncertainties are characterized with rms values,

$$\mathrm{rms}(x) = \sqrt{\sum x_i^2/N}, \qquad (5)$$

where x_i form a sample of N independent observations of the variable x. In the simulations the Monte Carlo noise, i.e., the rms-value of $\Delta I/I$ resulting from the simulation procedure itself is in all cases below 2%. Because of the moderate optical depths and the use of both forced first scattering and peel-off methods, the errors are relatively uniform, the relative uncertainty still being somewhat higher in regions of low column density. In simulations of actual observations, additional noise is added to these maps in order to simulate the measurement errors. At low intensities the added noise component is always large compared with the Monte Carlo noise. At high intensities the Monte Carlo noise becomes dominant, but is still below ∼2% when the surface brightness exceeds the average intensity of the map.

In the radiative transfer calculations the model clouds can be scaled arbitrarily, and the obtained surface brightness is affected only by the column density. As an example, we scale all the model clouds to a size of $L = 1.0$ pc, and rescale the

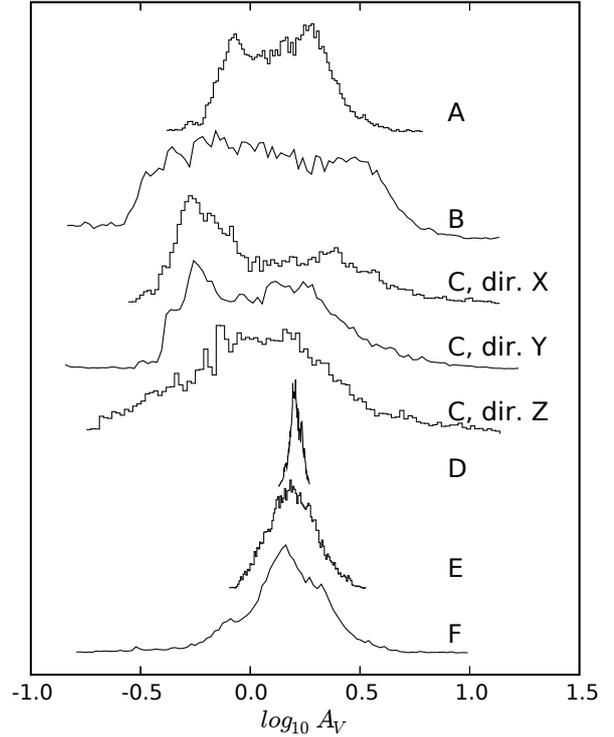densities to obtain model clouds of different opacity. In the case of the 125^3 cell models D–F one cell would correspond to 0.004 pc (825 AU) and, if that cloud were at the distance of 415 pc, the pixel size would be one arc second.

Initially we assume a mean density of 10^3 cm^{-3}. This results in an average column density of 3.1×10^{21} cm^{-2} which, in the case of the normal Milky Way dust ($R = 3.1$), corresponds to 1.6 mag of visual extinction. The actual range of extinctions depends on the inhomogeneity of the models. Figure 3 shows the A_V distributions for the six model clouds in the case of $\langle n \rangle = 10^3$ cm^{-3}. For example, in the model D practically all lines of sight have extinction below 3 mag, while in the model C the maximum extinction is over 17$^{\mathrm{m}}$. Later we consider also some models with twice as high density and $\langle A_V \rangle = 3.2$ mag. In the figures we will use visual extinction instead of column density. Because the dust properties are constant within each model, the ratio between A_V and true column density is also always constant.

In the simulations the model cloud is illuminated by an isotropic radiation field, with intensities calculated according to Mathis et al. (1983) model of the ISRF. However, since the observed surface brightness is directly proportional to the intensity of the incoming radiation, the simulations can be re-scaled for any spectrum of the background radiation. Based on DIRBE data Lehtinen & Mattila (1996) estimated the near-infrared intensity of the ISRF to be higher by some 50%. In our analysis this higher intensity level would only affect the estimated observing times, which would be shorter by a factor of ∼2.

Dust properties are based on Draine (2003) and we use the data files available on the web[2]. In most cases we assume normal Milky Way dust for which the ratio of total to selective

---

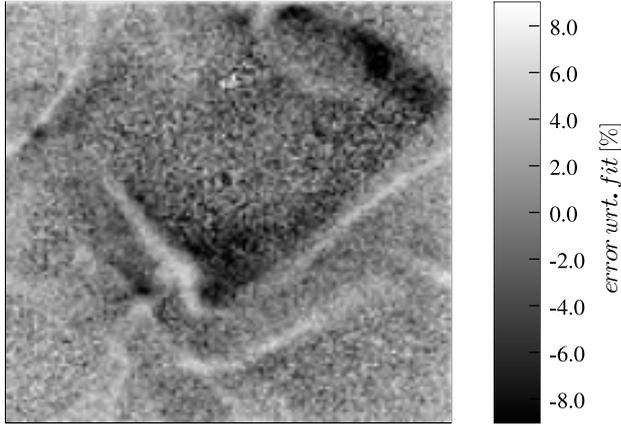[2] http://www.astro.princeton.edu/~draine/dust/

Fig. 4. A map of the difference between the simulated surface brightness and the prediction based on a curve fitted according to Eq. (1). The cloud is model C with $\langle A_V \rangle = 1.6$. The figure shows the shadowing effects that are caused by regions of moderate optical depth.

extinction is $R_V = A_V/E(B - V) = 3.1$. For the scattering function we use the tabulated scattering phase functions that are available on the web. In Sect. 4.2.2 we will examine the effect of dust with $R_V = 4.0$ or $R_V = 5.5$, and the effect of spatially varying dust properties. In those cases the scattering calculations are based on the Henyey-Greenstein scattering functions (Henyey & Greenstein 1941) and the asymmetry parameters g calculated for the different R_V cases.

4. Results

In this section we examine how the correlation between cloud column density and the observed NIR surface brightness depends on factors like the cloud structure, the average optical depth and the dust properties. The methods of Sect. 2 are used to convert surface brightness measurements into column density estimates. We study the accuracy of the obtained column density maps and examine how the results could be improved with detailed radiative transfer modelling or by the use of colour excess data from background stars.

4.1. Correlation between scattered light and column density

If NIR scattered light is to be used for a reliable estimation of the column density, the relation between these quantities should be universal or, when differences occur, those variations should be taken into account using the available observations. In the following we study how the results are affected by the cloud properties.

Figure 4 shows the difference between simulated surface brightness and predictions of Eq. (1) that best fits the points (N, $I_\nu(H)$). The differences are dominated by systematic features that are connected with the cloud structure (see Fig. 2b) and arise from the attenuation of the radiation field before reaching the line of sight in question. This is most noticeable in the case of thick filaments. Toward the cloud centre the filaments appear darker than on the outer side that is subjected to a stronger radiation field. When the method of Sect. 2 is applied, this effect will probably dominate the pixel-to-pixel errors in the derived column density maps. In Fig. 5 the relative rms-errors, rms($\Delta I_\nu/I_\nu$), are plotted for selected models as functions of the true A_V values.

A second source of uncertainty is the fact that parameters of Eq. (1) might vary from source to source in an unpredictable
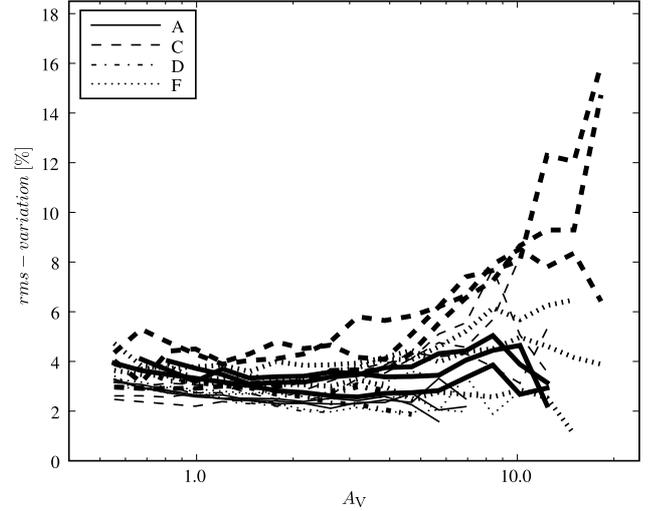

Fig. 5. Relative rms-variation between between the simulated H-band surface brightness and the average curve based on Eq. (1), for models A, C, D, and E, where the mean visual extinction is scaled to either $A = 1.6$ (thin lines) or $A = 3.2$ (thick lines). For each model separate curves are shown corresponding to observations from three different directions (X, Y, and $D1$). This plot illustrates the amount of variation in the surface brightness of scattered light for a given line-of-sight column density.
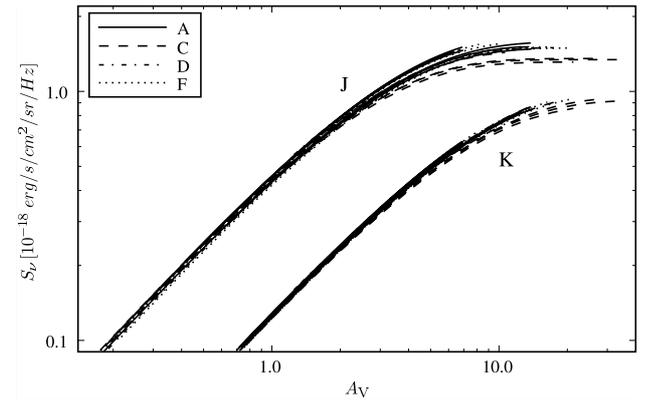

Fig. 6. Curves of Eq. (1) fitted to data from selected models (models as in Fig. 5). The lower curve is for the K band and the upper curve for the J band. Each curve is drawn for the range of A_V values found in the corresponding model and direction of observations.

fashion. This could produce more systematic errors, such as a bias in all column density values or in the ratio between low and high column densities. We will later study to what extent such variations can be corrected using the observations themselves. Here we consider only the amount of variation caused by the A_V and the cloud structure. Figure 6 shows for some models the fitted curves of Eq. (1). The deviation from the average behavior is largest for the most optically thick model C. In this case the maximum extinction is high, over 30 mag. The shadowing produced by such optically very thick regions is visible even at lower A_V as relatively lower surface brightness.

In Fig. 7 shows scatter plots of surface brightness versus A_V for data combined from all six model clouds and three viewing directions (X, Y, and $D1$). The two frames correspond to the two different values of average extinction. The figure shows the total expected dispersion between surface brightness and A_V. It therefore illustrates the accuracy of a column density estimate based on the surface brightness of NIR scattered light.
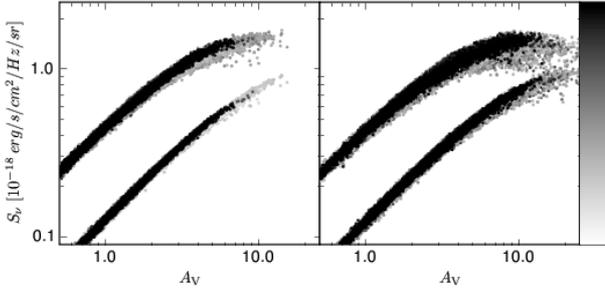
Fig. 7. Scatter plots of surface brightness versus A_V. The plot combines data from all six model clouds and three directions of observation (X, Y, and $D1$). The two frames correspond to average visual extinction $\langle A_V \rangle = 1.6$ and 3.2. The colour scale is linear with respect to the density of points.

In real clouds high densities are limited to the clouds inner parts and are, therefore, never subjected to full, unattenuated external field. On the other hand, the MHD turbulence simulations employ periodic boundary conditions and large densities may be found near the "surface" of our model clouds. Furthermore, when we look at a model perpendicular to its sides (direction X, Y, or Z), we have sightlines with high densities on both the front and back side of the cloud. This means that in our simulations the scatter in the relation between surface brightness and column density is larger than in real clouds. We examined the magnitude of this effect for all the models with $\langle A_V \rangle = 3.2^m$. We masked out five-pixel-wide map borders and sightlines where the density on the front surface exceeded one third of the average density of the cloud. The scatter with respect to the analytical fit of Eq. (1) decreased by less than ~10%, showing that edge effects will have only a small influence on the results.

4.2. Accuracy of the estimated column density

In this section we use the method of Sect. 2 to convert simulated surface brightness maps into estimates of column density. We examine the effects that column density distribution and dust properties can have on such estimates.

There are several possible ways of using Eq. (1). One could use either a generic set of parameters a and b, or try to improve the parameter values using the observations themselves. For example, the correct ratio of a-parameters can be determined directly from observations at low column densities. In practice such a procedure might be necessary, because, for example, the spectrum of the illuminating radiation field might not be known beforehand with sufficient accuracy. These possibilities are examined further in Sect. 4.3 and in Appendix A. In this section we use a single set of values of the a and b constants that are obtained as the average of all model runs. As shown by Fig. 6, there is little variation between the different models, except for the model C with $\langle A_V \rangle = 3.2$, where the presence of optically thick knots has changed the relation even for sightlines with $A_V \sim 10$. This extreme model was excluded from the calculation of the average parameters.

We will also consider the effect of random noise to simulate the effect of observational errors, assuming signal to noise ratios of 20, 15, and 7 for the J, H, and K bands. We will take the ISAAC/VLT instrument as an example. Assuming a $0.6''$ resolution the total integration time (on-source) is approximately 50 h. In the following we assume that one pixel in the simulated maps corresponds to $0.3''$. The S/N ratio per pixel is lower by a factor of two, but in the subsequent tests we smooth the maps
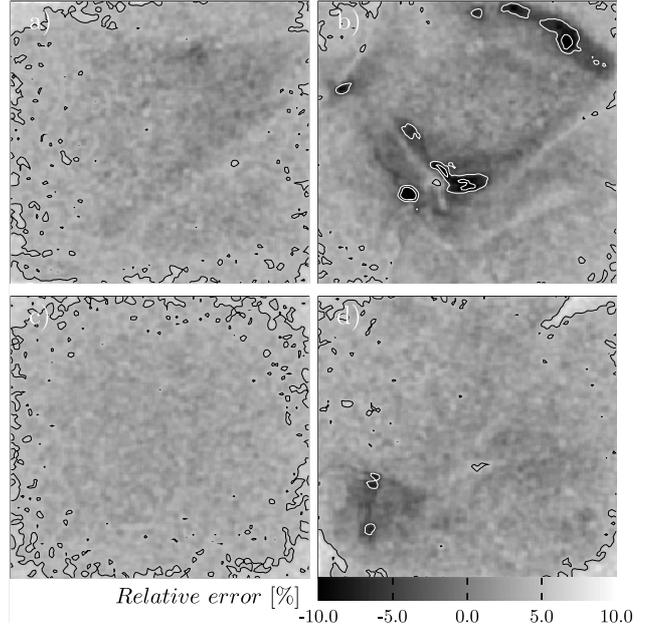

Fig. 8. Maps of relative error of column density estimates in the case of the models shown in Fig. 2. The average extinction is 1.6 mag (see Fig. 3), the input maps are convolved with a beam with fwhm equal to two pixels, and no observational noise is added. The contours are drawn at the levels of $\pm 5\%$ and $\pm 10\%$. The plots show the total projected area of model clouds.

down to the resolution of two pixels. Consequently, in the tests the actual noise corresponds to the S/N ratios quoted above. The ratios were calculated for the expected average surface brightness of a cloud with $\langle A_V \rangle = 1.6$. In the denser regions and in the more optically thick clouds the relative noise will be significantly lower. Compared with Padoan et al. (2006) our integration times are longer, mainly because of the lower average column density of the models.

The accuracies derived in this section reflect the intrinsic variation between clouds with different density structure and different optical depth, and the effect of observational errors.

4.2.1. Effect of column density distribution

Figure 8 shows some maps of the error in the column density estimates when no observational noise is added. The input maps were convolved with a beam with fwhm equal to twice the pixel size so that the estimated Monte Carlo noise is brought down close to one per cent. Because the S/N ratio is the same for all bands, the accuracy is limited mostly by the saturation of the surface brightness and can be improved by giving a larger weight to the longer wavelength data. In this case the optimal ratio was 1:3:12 for the weighting of J-, H-, and K-band data. In the case of actual observations, the different S/N ratios will change the optimal ratio. One would also expect the overall rms error to be reduced if the weight of the shorter wavelengths were decreased according to the extinction. In practice this was found to yield only little improvement, and the column density predictions were calculated using the constant weighting ratio. The errors were largest in the case of model C, where, after the smoothing of the maps, the maximum visual extinction was 14 mag. The maximum error was 23%. The average relative rms error was only 1.7%, large part of this number still being noise from the simulation procedure. This is to be expected, since the majority of sightlines are optically thin and the surface brightness
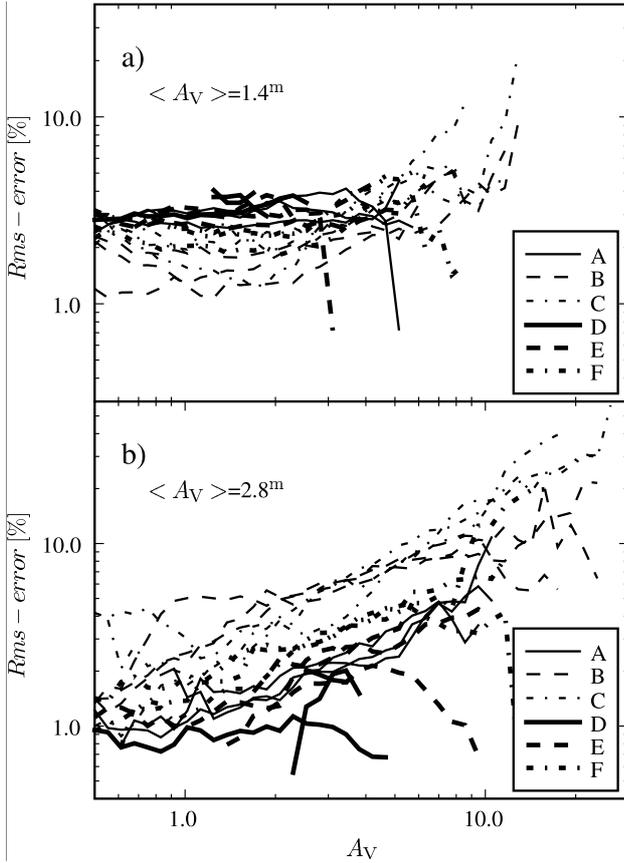
Fig. 9. Rms-error of column density estimates as a function of the line-of-sight visual extinction. The plot includes results for all six model clouds, for three different directions of observation (X, Y, and $D1$). The frames correspond to the two values of average visual extinction.

Fig. 10. Rms-error of column density estimates as a function of A. The plot includes results for all six model clouds and for three different directions of observation (X, Y, and $D1$). Observational noise was added to the input maps (see text). The frames correspond to the two values of average visual extinction.

is directly proportional to the column density. In model C the largest deviations are found in dense filaments. The other clouds are more homogeneous, and the errors reflect large scale gradients in the strength of the radiation field: The column density is systematically over-estimated close to the cloud borders.

In Fig. 9 we show the average rms-error of the column density estimates as a function of A_V. As before, the predictions are calculated using the average values of the parameters a and b. In models with $\langle A_V \rangle = 1.6$ the errors remain mostly below 10% with the exception of model C where, as already mentioned, the largest error is ~23%. In the optically thicker clouds, $\langle A_V \rangle = 3.2^m$, the errors are larger for all sightlines, as the shadowing by optically thick regions causes fluctuations in the strength of the radiation field. However, below $A_V \sim 10^m$ the errors are at most 10%. Above $A_V \sim 20^m$ the average errors increase close to 50%.

Next, we add noise to the surface brightness maps to simulate the observational uncertainties. The S/N ratios are 20, 15, and 7 for the J, H, and K bands respectively, when calculated for the average surface brightness of the $\langle A_V \rangle = 1.6$ maps and the maps are smoothed to a resolution of two pixels. The weighting of the different bands is kept the same as before. The results are shown in Fig. 10. The main effect of the added noise is a decrease in the accuracy at small column densities. The relative errors are ~10% at $A_V = 0.5^m$, decrease until $A \sim 4^m$, and again increase at higher column densities as in Fig. 9. A good signal-to-noise ratio should be particularly important at high opacities where, due to the saturation of the surface brightness values, a small change in surface brightness corresponds to a large change
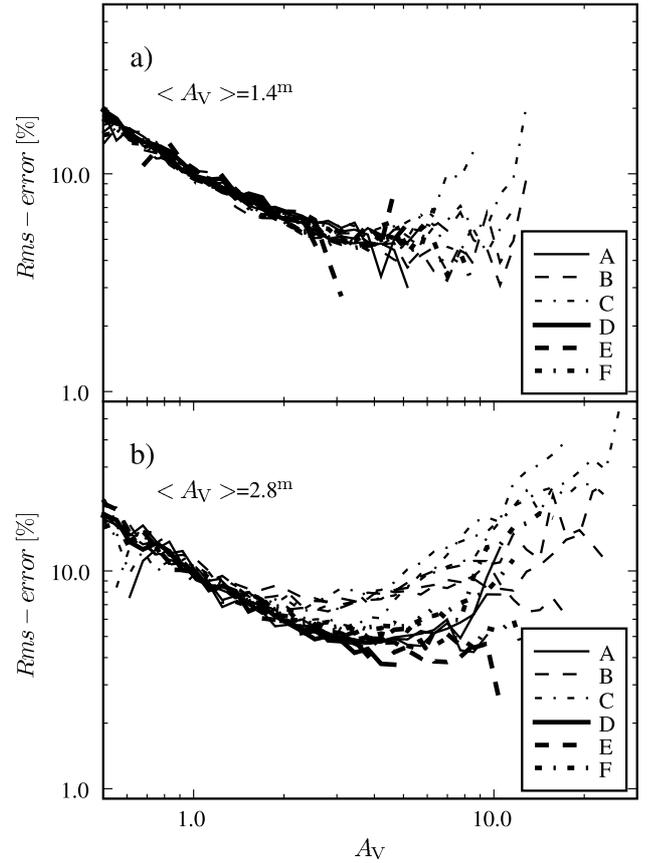
in column density. However, in these regions the S/N ratios are already very high and, beyond $A_V \sim 8^m$, Figs. 9 and 10 are practically identical. Figure 11 shows maps of the estimated column density maps for the four models of Fig. 2.

The column density distribution also depends on the resolution of the observations or, in our case, the resolution of the simulations. The discretization of the cloud models could affect the results if individual cells were optically thick *and* if a finer discretization resolved significant density variations within the original cells. The largest density contrast is found in model C. When the cloud has an average visual extinction of $\langle A_V \rangle = 3.2^m$, the J-band optical depth of the densest cell is ~1.3 and 99.99% of the cells have optical depth below $\tau_J = 0.5$. The maximum optical depth is smaller for the other bands and models and, naturally, for the clouds scaled to $\langle A_V \rangle = 1.6$. Therefore, discretization is not expected to produce errors that could affect our results. This was still checked using the model F. The original MHD simulation was done on a grid of 256^3 cells and based on that we constructed three models consisting of 256^3, 125^3, and 64^3 cells. Radiative transfer simulations were repeated for all the three model clouds, and Fig. 12 shows the errors when column densities are estimated at the full resolution of each model. The larger differences at low A_V are caused by a difference in the Monte Carlo noise of the simulations. Otherwise, the accuracy of the column density determination is not seriously affected by the numerical resolution.
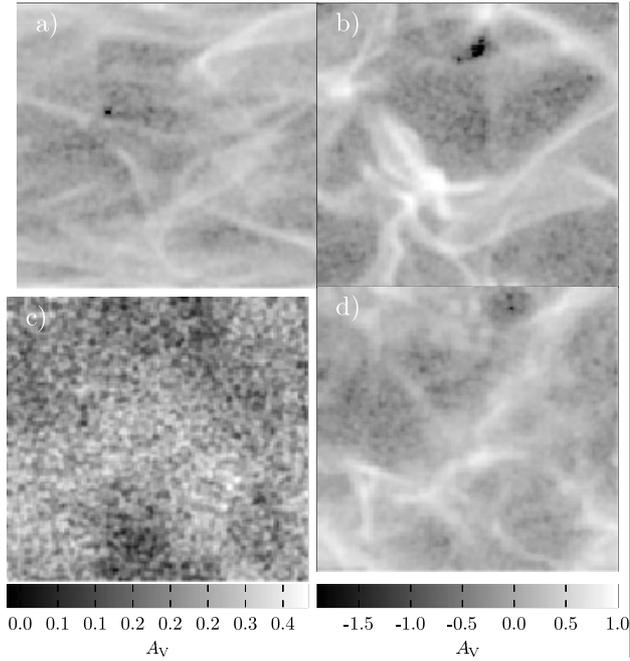
Fig. 11. Estimated column density maps of the four models (A, C, D, and E) of Fig. 2. The column densities are calculated based on surface brightness maps where observational noise is included (see text). The images show the logarithm of the column density, transformed into A_V. The frames a, b, and d share a common colour scale. The model D has a much smaller range of column densities (see Fig. 3), and the frame c has a different colour scale.
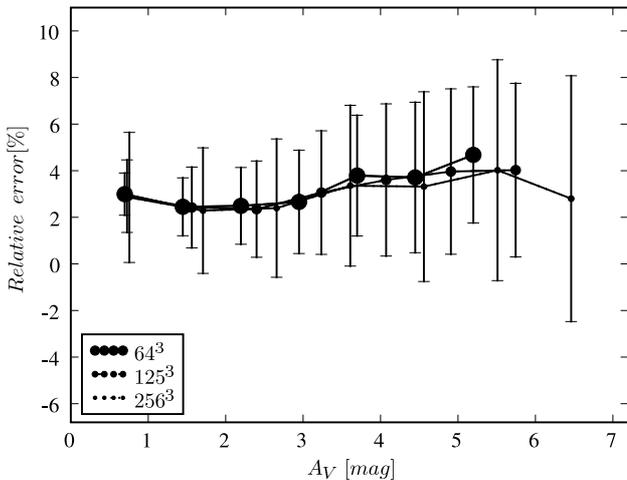

Fig. 12. The errors of the estimated column densities when model F is discretized into 64^3, 125^3, or 256^3 cells. The estimates are based on average parameters derived from all models with $\langle A_V \rangle = 1.6^m$ and $\langle A_V \rangle = 3.2^m$. The points show the average bias in different A_V intervals and the errorbars correspond to the 1-σ variation within each interval. At low A_V part of the differences is caused by the Monte Carlo noise of the simulations, which was higher for models of higher resolution.

4.2.2. Effect of radiation field and dust properties

In deriving the column densities we have so far assumed that model parameters a and b have already been determined from other models illuminated with similar external radiation field and containing dust with exactly the same scattering properties. In reality, both radiation field and dust properties can be subject to significant variations.

If the total level of the incoming radiation is underestimated, the column density is correspondingly overestimated. Below $A_V \sim 10^m$ the surface brightness is directly proportional to the external field so that an error in the assumed intensity of the radiation field results in similar relative error in the column densities. This is a constant factor and does not affect relative accuracy between map positions. An error in the assumed spectrum, i.e., in the intensity ratio between different bands, can result in different kinds of errors, especially if the bands are weighted differently, according to the local S/N-ratios. However, observations of optically thin sightlines can be used to correct for changes in the spectrum and, partially, changes in dust properties.

We repeated simulations of model C using dust with $R_V = 4.0$ and $R_V = 5.5$. The dust parameters were taken from Draine et al. (2003). The J- and H-band intensities were plotted against the K-band intensity, and Eq. (3) was fitted to the data. The parameters a_K and b_K were kept constant using the previous values that were derived assuming $R_V = 3.1$. In the NIR the shape of the extinction curve remains rather constant, and the main effect results from differences in the absolute values of the absorption and scattering cross sections. In the optically thin regime the product $a \times b$ is the slope of the relation between surface brightness and column density. Since these ratios of $a \times b$ in different bands can be determined from the data itself, no a priori assumption needs to be made about the spectrum of the external radiation, and some of the uncertainty caused by unknown dust scattering properties is eliminated. However, because the value of the product $a_K \times b_K$ must be assumed, the column density estimates may be at error by a constant factor as discussed above. The situation is worse at high column densities because we cannot directly determine the column density at which the saturation of the surface brightness values starts. While the ratios between the b parameters can be recovered from the data, the value of an individual b parameter must be assumed a priori. If the dust extinction cross sections are different from the assumed one, the saturation begins at a higher or lower column density than expected, and all column density estimates of high extinction sightlines are correspondingly erroneous. Moreover, if the radiation field is stronger than expected, the column densities will be overestimated in the non-linear part of Eq. (1). If the surface brightness exceeds the expected asymptotic value, represented by the parameters a, no solution can be found. However, in such a case the peak surface brightness can be used to correct the value of a_K.

Figure 13 shows the bias and statistical noise in the cases of $R_V = 3.1$ or $R_V = 5.5$. The b_K and a_K parameters correspond to a case $R_V = 4.0$, and the other parameters have been re-estimated from the plots of the J- and H-band intensity versus the K-band intensity. In frame a the radiation field is the same as before. No additional observational noise was included. The surface brightness of the scattered light increases with the R_V value of the dust. Therefore, for $R_V = 5.5$ the column densities are overestimated and on the non-linear part the systematic error increases rapidly as the line-of-sight extinction exceeds $A_V \sim 10^m$. The maximum observed surface brightness was not used to correct the value of the parameter a_K. In the case $R_V = 3.1$ the column densities are underestimated, but errors are smaller, being $\sim$20% or less for $A_V \sim 10^m$.

In frame b the radiation field was increased by 30% relative to the value assumed in the column density derivation. At higher column densities, and especially in the case with $R_V = 5.5$, the column densities would be either seriously overestimated or no value could be obtained from Eq. (1). Therefore, the analysis was done using a corrected a_K value that was set to the
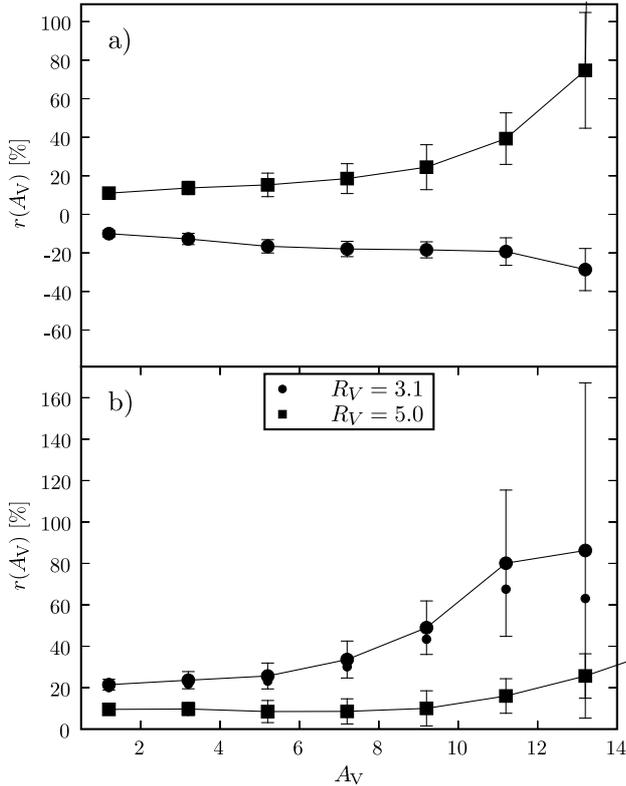
Fig. 13. Effect of a change in dust properties and/or field strength on the column density estimates. The plots show the bias and scatter in the estimates when dust properties are assumed to correspond to R_V = 4.0, while they in reality correspond to either R_V = 3.1 or R_V = 5.5. In frame b the radiation field is also 30% higher than assumed in the column density derivation, and the parameter a_K is re-estimated based on the maximum surface brightness. The small circles show the result in the case of R_V = 3.1 without re-evaluation of parameter a_K.

the intrinsic colours of the stars. The resolution of the resulting column density map is much lower than the resolution of the surface brightness maps. This information can, however, be used to assist the use of surface brightness measurements. The combination of the two methods is interesting because, while both rely on absorption and scattering by dust particles, their actual dependence on the dust properties is different. Furthermore, the colour excess method is independent of the local radiation field. This makes it possible to take into account any radiation anisotropies in the studied field. Conversely, differences in the two column density estimates serve as a sensitive indicator of variations in dust properties and the radiation field.

In the following we use simplified simulations of the colour excess method where extinction maps are calculated with the NICER method (Lombardi & Alves 2001). Stars are placed at random locations behind the model cloud and their extinction is proportional to the true column density. The magnitude distribution follows a linear (mag, $\log N$) relation with a slope of 0.35. A random error of 0.12 mag is added to each band in order to simulate photometric errors and the variation in the intrinsic colours of the stars. The resulting dispersion in the colours is similar to or slightly smaller than the scatter found in 2MASS data. For simplicity, the same noise was applied to all stars. Faint stars are removed when their magnitudes exceed some limit m_K in the K-band, m_K + 0.85 magnitudes in the H-band, or m_k + 1.5 mag in the J-band. The m_K limit determines the remaining number of stars.

The comparison of extinction and surface brightness gives a way to determine all the parameters of Eq. (1) directly from observations. This was tested on model C, using the 128 × 128 maps and adding observational noise as in the previous section. The upper frame of Fig. 14 shows the accuracy of the extinction maps that were derived from simulated colour excess observations and were averaged with a Gaussian with *FWHM* equal to 7 pixels. The number of background stars over the whole map was ∼2000. The lower frame shows the results for the surface brightness method together with errors calculated for individual pixels. The parameters a and b were either average values of all model clouds, including both models with $\langle A_V \rangle = 1.6^m$ and $\langle A_V \rangle = 3.2^m$ (see Sect. 3.2), or were estimated through a comparison of surface brightness and extinction maps. The colour excess data did not significantly improve the accuracy of the surface brightness method. This is not surprising because the average parameters were based on simulations with correct dust properties and correct value of the background radiation field. On the other hand, Fig. 14 does show that by using the colour excess information similar accuracy can be reached even without any such a priori knowledge of the dust properties and of the radiation field. Extinction measurements are therefore useful to avoid assumptions about dust properties and radiation field intensity in the application of our method. The column density map obtained with our method still has a much better spatial resolution that the extinction map itself, seven times better in this case.

In the previous discussion, the colour excess information was used globally, through the model parameters a and b. Alternatively, one could combine the extinction map and the column density map obtained from our method, at the lower resolution of the extinction map. Spatial variations in the ratio of the maps could serve as an indicator of changes in dust properties or in the strength of the local radiation field. To test these possibilities we modified the model C ($\langle A_V \rangle = 1.6^m$), first re-examining the effect of changing dust properties. The fractional abundance of dust with R_V = 3.1 was set to depend on local density

maximum observed K-band intensity. Such a correction assumes that maps contain at least one optically thick region. Because we have assumed that the radiation field is underestimated, the column densities are overestimated for all sightlines and for both dust models. However, in the case of dust with R_V = 5.5 the errors are, in fact, much smaller than before. Apparently the correction of the parameter a_K compensated also for the higher than expected dust scattering efficiency. On the other hand, for dust with R_V = 3.1 the corrected a_K value does not improve the estimates. Without clearly saturated regions the maximum surface brightness is a poor measure of a_K. In that case the parameter values can be corrected only by other methods, for example by comparison with an extinction map (see Sect. 4.3). In some cases the accuracy can be improved by more detailed modelling of the observed source. This possibility is discussed further in Appendix A.

4.3. Use of extinction measurements

Observations of NIR surface brightness will automatically give photometry for a large number of background stars. The colour excesses of the stars can be converted into estimates of the clouds column density (Alves et al. 2001; Lombardi & Alves 2001; Cambrésy et al. 2002). Each star can be treated as a probe of the extinction along individual, very narrow sightlines. Usually the results are spatially smoothed to give a map of extinction at lower resolution. Averaging is required because of the scatter in
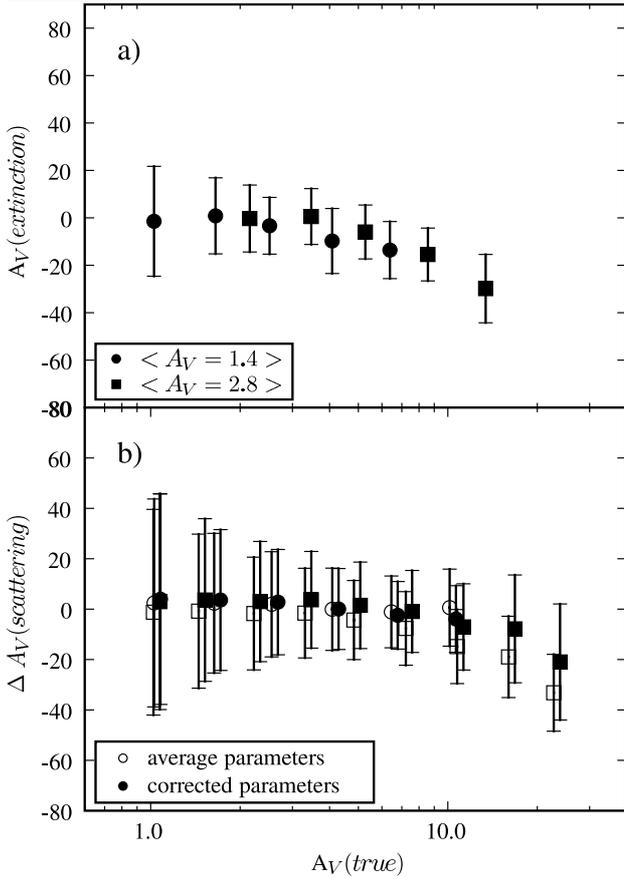
Fig. 14. *Upper frame*: errors in the simulated extinction map. Plots are shown for two versions of model C, with average visual extinction 1.6 (circles) or 3.2 mag (squares). The resolution of the extinction map corresponds to a *FWHM* equal to seven map pixels. *Lower frame*: accuracy of the column density estimates based on NIR scattering. Results are shown for the two versions of the model C. The parameters are either the average values from all models (six clouds, three viewing directions and two scalings of average column density; open symbols) or were determined by correlating surface brightness against column densities estimated using the colour excess method (solid symbols).

according to the function $f = n/(2000 + n)$. Dust with $R_V = 5.5$ was given relative abundance $1 - f$. Column densities were estimated with both methods (Fig. 15). The colour excess method gives very accurately the correct average visual extinction but, with 2000 simulated background stars, the map has significant noise. When the surface brightness method is applied using parameters tuned for $R_V = 3.1$ dust, the column densities of the same regions are significantly over-estimated. The ratio of the two estimates reflects, therefore, both resolution effects and the changes in dust properties. The intensity ratios of the NIR bands would, of course, also directly show that the assumption of either the dust properties or the radiation field is not correct. As above, the extinction map is used to re-evaluate the average global parameters for the surface brightness method. The resulting map is shown in Fig. 15c. The highest column densities are slightly overestimated but the map is morphologically extremely accurate. As before, the surface brightness data contained observational noise. In Fig. 15 all the three maps are smoothed to a resolution of six pixels, but the signal-to-noise ratios would allow a much higher spatial resolution for the map that was based on the surface brightness data. Extinction measurements could also be used in the creation of a detailed radiative transfer model of the source (see Appendix A). That would

be particularly useful in the case of a strongly anisotropic radiation field.

Local radiation sources may complicate the derivation of the column densities. Depending on the spectrum of these sources, it may be difficult to deduce their presence based on surface brightness data only. This is true especially if the true column density is low and the surface brightness itself is not anomalously high. In that case the sources could lead to significant overestimation of the column density. In the following we examine how such errors manifest themselves in the estimated column density maps and to what extent the colour excess data can be used to correct the results. We added to cloud *C* three point sources, each with a 4000 K black body spectrum. The *K*-band luminosities were 1.5×10^{19}, 3.1×10^{19}, and 6.2×10^{19} erg/s/Hz. Figure 16a–c shows the surface brightness maps for each source separately, excluding direct radiation from the source. The lower frames show again the true column densities, the NICER estimates (using 2000 background stars), and the estimates based on scattered light, all convolved with a beam with *FWHM* ~ 6 pixels. In observations, the presence of the strongest source would be obvious, based on the presence of the point source, high surface brightness values in excess of the ISRF intensity, and comparison with the NICER map. The second source can still be seen by plotting the difference of the two column density estimates. In the surface brightness method (using default parameters) the estimated column density at the position of source 2 is twice the correct value. However, the effect of this source is very local. At the distance of 6 pixels the error is still $\sim100\%$ but falls below 50% at the distance of 12 pixels. The weakest source is outside dense regions and therefore does not produce A clear peak in the surface brightness or estimated column density. There is, however, a diffuse area ($\sim1\%$ of the whole map) where the column density is overestimated by $\sim30\%$. Because the area has low extinction, $A_V < 4$, the noise is relatively high in the NICER map, and it would be difficult to detect the effect of this source in actual observations.

5. Discussion

Observations of scattered NIR light provide a means to map large areas of interstellar clouds with very high spatial resolution. Our simulations showed that one can reach average pixel-to-pixel accuracy better than 10% as long as the maximum extinction is below $A_V \sim 15^m$. High absolute accuracy requires that the parameters of Eq. (1) can be determined with similar precision. This requires knowledge of both the radiation field and the dust properties. Fortunately, the NIR observations will automatically give colour excess data for a large number of background stars. Comparison of surface brightness data and the colour excess data provides a direct way to determine the parameters of Eq. (1). Therefore, the column density estimation can be carried out with little a priori information. This is particularly important regarding the radiation field because its intensity is usually unknown and cannot be easily determined. On the other hand, the NIR dust properties are generally believed to be rather constant among sources of similar type. If the conversion between surface brightness and column density is done with incorrect parameters, the absolute scaling and the relative values, as a function of position or column density, will be incorrect. However, the derived column density maps are still usually morphologically accurate (see, e.g., Fig. 15).

The use of Eq. (1) contains the assumption that the intensity of the radiation field and the dust properties are constant within the cloud. Spatial variations of dust properties were examined in
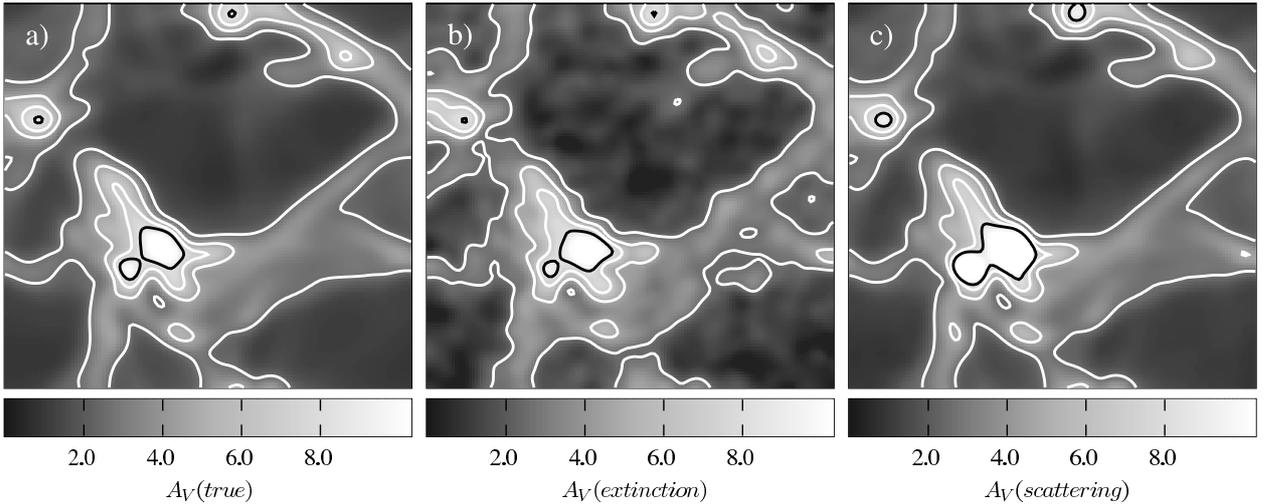
Fig. 15. Model containing variable dust properties, $R_V = 3.1$ in low density regions and $R_V = 5.5$ in high density regions. The frames are: *a*. True A_V, *b*. A_V based on colour excesses of ~2000 background stars, and *c*. A_V based on scattered surface brightness. All maps have been smoothed to a resolution of six map pixels.
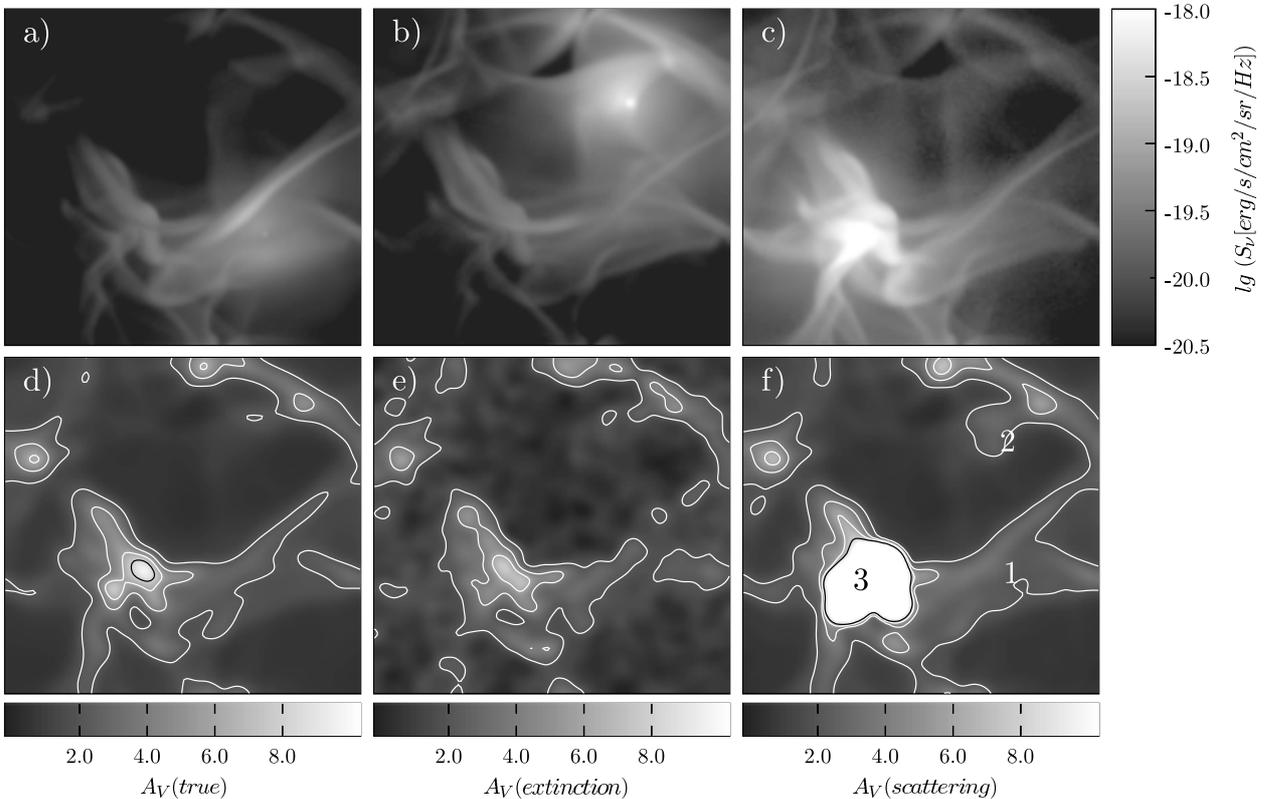

Fig. 16. Frames **a)**–**c)**: *H*-band surface brightness maps for each of the three point sources that were added to model cloud *C*. Frame **d)**–**f)**: column density estimates for model C containing three point sources. The maps show the true column density, estimates based on NICER method and estimates based on scattered surface brightness. Note that the colour scale is logarithmic in the upper frames and linear in the lower frames.

Sect. 4.3. In particular, Fig. 13 showed that although variation between dust with $R_V = 3.1$ and $R_V = 5.5$ can introduce visible changes in the estimated column density maps, the variations are still only at the 10% level. Our simulations showed that as long as the clouds are not very optically thick, $A_V \sim 15^m$ or below, the errors caused by large scale radiation field gradients are ~10% or below. The effect was visible mainly towards the edges of relatively homogeneous clouds (see Fig. 8).

At large scales the spatial variations in the dust properties and the radiation field can be recognized with the help of background stars. An extinction map that is based on background stars will have a much lower resolution than the surface brightness maps. Furthermore, because the parameters of Eq. (1) can only be determined using correlations over large areas, rapid spatial variations in dust properties may not be taken fully into account. Nevertheless, the comparison of extinction and surface brightness maps will give indication of those variations. Some effects can be recognized and corrected based on surface brightness data itself. This is discussed further in Appendix A, where we examine the possibility of improving the accuracy of the

column density estimates through detailed radiative transfer modelling. The effects resulting from radiation field and dust property variations are examined further in Appendix B.

We have assumed that the observed surface brightness is caused entirely by dust scattering. The contribution from emission lines is small but the role of NIR dust emission remains uncertain. At low A_V sightlines a significant part of the surface brightness could be caused by emission from very small grains or possibly PAHs (Flagey et al. 2006). If, as it seems likely, the emission is restricted to regions of low extinction and mainly to $\lambda \gtrsim 2\,\mu m$, it will not cause serious problems for the column density estimation. If Eq. (1) is modified to accommodate the additional emission component, colour excess data of background stars can still be used to derive the relation between K-band surface brightness and column density for higher A_V. This question is discussed further in the Appendix B.4. Further modifications to Eq. (1) will be needed if the surface brightness of the background sky is not negligible. At high galactic latitudes the extragalactic infrared background is the main background component. If completely ignored, it could cause systematic errors again at the level of 10% percent (see Appendix B.4.3). However, if the parameters of Eq. (1) are determined through comparison with extinction data, most of this error is already automatically eliminated.

The scattered light traces the distribution of dust, and the total column density can be estimated by assuming a constant gas-to-dust ratio. Conversely, the scattered surface brightness provides a way to study the relative distribution of gas and dust. In the NIR one can easily reach sub-arcsecond resolution, which, at the distance of the closest star forming regions corresponds to only ~ 100 AU. Comparison with interferometric observations of suitable molecular tracers might reveal entirely new phenomena, such as the clustering of dust grains within turbulent flows (Padoan et al. 2006).

6. Conclusions

We have examined the use of scattered NIR surface brightness as a high resolution tracer of the structure of interstellar clouds. Column densities are estimated using the J, H, and K bands. In the optically thin case the observed surface brightness is directly proportional to column density. In clouds of moderate optical thickness, A_V below $\sim 15^{\mathrm{mag}}$, the saturation of the NIR surface brightness can be corrected, and reliable estimation of column densities is still possible. We have studied how the column density estimation is affected by cloud structure, optical depth, and dust property variations. In the numerical models the absolute accuracy of the estimated column densities is better than $\sim 20\%$. Large variations in the radiation field or dust properties can cause large errors, if not corrected for. However, even in those cases the errors are mostly systematic, and the relative errors between map pixels are significantly lower than the systematic errors.

Sensitive observations of the surface brightness will automatically provide colour excess data on background stars that can be used as a largely independent measure of the column density. We showed that by combining the two methods most of the errors caused by anomalous radiation field or dust properties can be easily corrected, resulting in a reliable column density map with significantly higher resolution than is possible with colour excess data alone. Conversely, the comparison of the two column density estimates can give important information on the radiation field and dust property variations within the cloud, and even give hints on its three-dimensional structure.

References

Aharonian, F., Akhperjanian, A. G., Bazer-Bachi, A. R., et al. 2006, Nature, 440, 1018
Alves, J., Lada, C., & Lada, E. 2001, Nature, 409, 159
Arendt, R. G., Odegard, N., Weiland, J. L., et al. 1998, ApJ, 508, 74
Bernard, J. P., Boulanger, F., Désert, F. X., et al. 1994, A&A, 291, L5
Black, J., & van Dishoeck, E. F. 1987, ApJ, 322, 412
Boudet, N., Mutschke, H., Nayral, C., et al. 2005, ApJ, 633, 272
Cambrésy, L. 1999, A&A, 345, 965
Cambrésy, L., Boulanger, F., Lagache, G., & Stepnik, B. 2001, A&A, 375, 999
Cambrésy, L., Beichman, C. A., Jarrett, T. H., & Cutri, R. M. 2002, AJ, 123, 2559
Cardelli, J. A., Clayton, G. C., & Mathis, J. S. 1989, ApJ, 345, 245
Cohen, M. 1994, AJ, 107, 582
Dupac, X., Bernard, J.-P., Boudet, N., et al. 2003, A&A, 404, L11
Draine, B. 2003, ApJ, 598, 1017
Dwek, E., Arendt, R. G., & Krennrich, F. 2005, ApJ, 635, 784
Egan, M. P., Shipman, R. F., Price, S. D., et al. 1998, ApJ, 494, L199
Flagey, N., Boulanger, F., Verstraete, L., et al. 2006, submitted [arXiv:astro-ph/0604238]
Foster, J., & Goodman, A. 2006, ApJ, 636, L105
Gómez, M., & Kenyon, S. J. 2001, AJ, 121, 974
Gordon, K. D., Witt, A. N., Rudy, R. J., et al. 2000, ApJ, 544, 859
Gorjian, V., Wright, E. L., & Chary, R. R. 2000, ApJ, 536, 550
Haikala, L. K., Mattila, K., Bowyer, S., et al. 1995, ApJ, 443, L33
Hauser, M. G., & Dwek, E. 2001, ARA&A, 39, 249
Hennebelle, P., Pérault, M., Teyssier, D., & Ganesh, S. 2001, A&A, 365, 598
Henyey, L. G., & Greenstein, J. L. 1941, ApJ, 93, 70
Juvela, M. 2005, A&A, 440, 531
Juvela, M., & Padoan, P. 2003, A&A, 397, 201
Juvela, M., Padoan, P., & Nordlund, Å. 2001, ApJ, 563, 853
Juvela, M., Padoan, P., & Jimenez, R. 2003, ApJ, 591, 258
Kelsall, T., Weiland, J. L., Franz, B. A., et al. 1998, ApJ, 508, 44
del Burgo, C., Laureijs, R. J., Ábrahám, P., & Kiss, Cs. 2003, MNRAS, 346, 403
Kramer, C., Richer, J., Mookerjea, B., et al. 2003, A&A, 399, 1073
Krugel, E., & Siebenmorgen, R. 1994, A&A, 288, 929
Lehtinen, K., & Mattila, K. 1996, A&A, 309, 570
Lehtinen, K., Russeil, D., Juvela, M., Mattila, K., & Lemke, D. 2004, A&A, 423, 975
Lehtinen, K., Juvela, M., Mattila, K., Lemke, D., & Russeil, D. 2006, submitted
Li, A., & Draine, B. 2001, ApJ, 554, 778
Lombardi, M., & Alves, J. 2001, A&A, 377, 1023
Mathis, J. S., Mezger, P. G., & Panagia, N. 1983, A&A, 128, 212
Mattioda, A. L., Allamandola, L. J., & Hudgins, D. M. 2005a, ApJ, 629, 1183
Mattioda, A. L., Hudgins, D. M., & Allamandola, L. J. 2005b, ApJ, 629, 1188
Mattila, K. 1970a, A&A, 8, 273
Mattila, K. 1970b, A&A, 9, 53
Mattila, K. 1976, A&A, 47, 77
Mennella, V., Brucato, J. R., Colangeli, L., et al. 1998, ApJ, 496, 1058
Nakajima, Y., Nagata, T., Sato, S., et al. 2003, AJ125, 1407
Nakamura, R., Fujii, Y., Ishiguro, M., et al. 2000, ApJ, 540, 1172
Ossenkopf, V., & Henning, T. 1994, A&A, 291, 943
Padoan, P., & Nordlund, Å. 1999, ApJ, 526, 279
Padoan, P., Bally, J., Billawala, Y., Juvela, M., & Nordlund, Å. 1999, ApJ, 525, 318
Padoan, P., Juvela, M., Goodman, A. A., & Nordlund, Å. 2001, ApJ, 553, 227
Padoan, P., Jimenez, R., Juvela, M., & Nordlund, Å. 2004, ApJ, 604, L49
Padoan, P., Juvela, M., & Pelkonen, V.-M. 2006, ApJ, 636, L101
Padoan, P., et al. 2006, in preparation
Reipurth, B. 1999, Herbig-Haro objects and their energy sources, Copenhagen University, 1999
Ridderstad, M., Juvela, M., Lehtinen, K., Lemke, D., & Liljestrom, T. 2006, A&A, 451, 961
Sellgren, K., Werner, M. W., & Allamandola, L. J. 1996, ApJS, 102, 369
Stepnik, B., Abergel, A., Bernard, J.-P., et al. 2003, A&A, 398, 551
Struve 1937, ApJ, 85, 94
Struve, O., & Elvey, C. T. 1936, ApJ, 83, 167
Wolf, M. 1923, Astron. Nachr., 219, 109
Zubko, V., Dwek, E., & Arendt, R. G. 2004, ApJS, 152, 211
Yusef-Zadeh, F., Morris, M., & White, R. L. 1984, ApJ, 278, 186

Online Material

Appendix A: Use of iterative radiative transfer modelling

The assumption of a uniform radiation field breaks down in optically thick regions (see Fig. 4b), and even in a homogeneous cloud the intensity gradients increase the errors of the column density estimates. These variations are related to the three-dimensional cloud structure and, therefore, can never be fully eliminated. A rough correction is possible, if the cloud structure along the line-of-sight can be ignored, and only the projected column density map is used. Variations in the radiation field can be estimated with radiative transfer calculations. An initial model cloud is created according to preliminary estimates of the column densities. In the line-of-sight the structure is not restricted by observations, and we start by assuming a Gaussian density profile with *FWHM* equal to one third of the cloud size. Radiative transfer calculations are used to produce maps of surface brightness, and the column densities of the model cloud are corrected iteratively, using the ratio of the observed and modelled intensities. The correction is done separately for each sight-line corresponding to a pixel in the maps.

The correction procedure was first applied to model F with $A_V = 1.6$ and on model D with $A_V = 3.2$. Cloud F is very inhomogeneous and, therefore, a correction without any knowledge of the line-of-sight structure is expected to be more difficult than for the more homogeneous cloud D (see Fig. 3). Since the iterative model fitting is somewhat time-consuming, the model clouds were downsized to 64^3 cells. The relative rms noise of the initial simulated maps was below 1%. This applies both to the initial "observed" surface brightness maps and the simulated maps produced during the iterations.

In Fig. A.1 we compare the resulting column density estimates with those obtained using Eq. (1) together with parameters a and b that were averages of the values obtained from the six models. As expected, the modelling works best for the cloud D. In that case estimates are free from bias and scatter is smaller than obtained with the default method. In the latter method, if we used exactly correct parameter values in Eq. (1), the bias would be removed but the scatter would remain unchanged. For model F the accuracy is rather similar for the two methods. The iterative modelling shows a systematic error 2–3%, probably as a consequence of the assumption of a smooth line-of-sight density distribution.

The use of Eq. (1) includes the effects of a clumpy cloud structure since the fit parameters are obtained from inhomogeneous models. On the other hand, it ignores any spatial variation on the plane of the sky. The iterative modelling worked differently, fitting the spatial variations but using a simplistic description for the line-of-sight density structure. Remaining errors in the column densities are a direct consequence of the true cloud structure differing from the smooth distribution used in the modelling. This is more clear in the case of model C for which error maps are shown in Fig. A.2. In this case the iterative modelling results in a much larger scatter (see Fig. A.3). The maps contain intriguing features, where the column density is either systematically overestimated or underestimated. The same regions can be easily recognized without knowledge of the true column density because, when column density is underestimated, the predicted J-band intensity from the iterative modelling is relatively higher and the K-band intensity lower than in the actual model C. This is caused by the fact that, because of the smaller saturation, the K-band intensity is more sensitive to changes in the column density. Comparison with Fig. 2b shows that the deviations are not necessarily associated with the largest column densities.
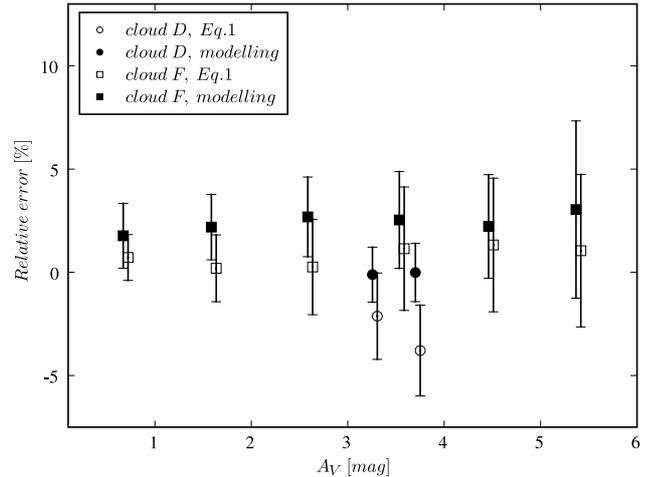

Fig. A.1. Comparison of the accuracy of column density estimates obtained with the analytical method (open symbols) and with detailed radiative transfer modelling (solid symbols). Results are shown for model D with $\langle A_V \rangle = 3.2^{\mathrm{m}}$ and for model F with $\langle A_V \rangle = 1.6^{\mathrm{m}}$. The plot shows the bias and the scatter with respect to the true column densities.

There could be several explanations for such deviations. First, a dense region close to the cloud surface could produce more surface brightness (especially in the J-band) and could result in an overestimation of the column density. Examination of the three-dimensional density distribution does not support this interpretation. The only region with clearly overestimated column density values is located close to the centre of cloud C. Similarly, the strongest negative features are caused by filaments that are relatively close to the cloud surface. The shape of the condensations may also play a role, the surface brightness being slightly higher when the material is distributed along a longer sightline. This agrees better with the structures seen in the cloud C. When the line-of-sight *FWHM* of the density distribution was used as a further free parameter, the previous fit results did indeed improve significantly (see Fig. A.3a).

The scattered surface brightness might also carry some information about the relative positions of the dense regions. If scattering occurs mostly in the forward direction, the surface brightness samples the average radiation field behind the clumps. In that case the clumps closest to the observer would have lower ratios between the surface brightness and the column density. However, this seems to be a very small effect. When model C is observed from the opposite direction, the resulting error maps do, within noise, exactly correspond to those shown in Fig. A.2. Finally, the deviations might be caused by the general lack of homogeneity, which would affect the way radiation can penetrate the cloud. This seems to be, at least partially, an explanation for the underestimated column densities in the cloud centre. This was tested in a qualitative way by using the density distribution of cloud D in the fitting of model C surface brightnesses. The initial line-of-sight densities were random (models D and C are completely independent runs), and the column densities corresponding to each map pixel were again optimized. The result is shown in Fig. A.3b. The scatter is now rather similar to what was obtained by using Eq. (1). The use of an inhomogeneous medium eliminates overestimated column densities in the central region. However, the negative features seen in Fig. A.2 do remain. These might be caused by the compactness of the emitting regions, as discussed above. Because the deviating regions are visible as excess in the simulated J-band maps, it should be possible to make a correction for those, for example by using
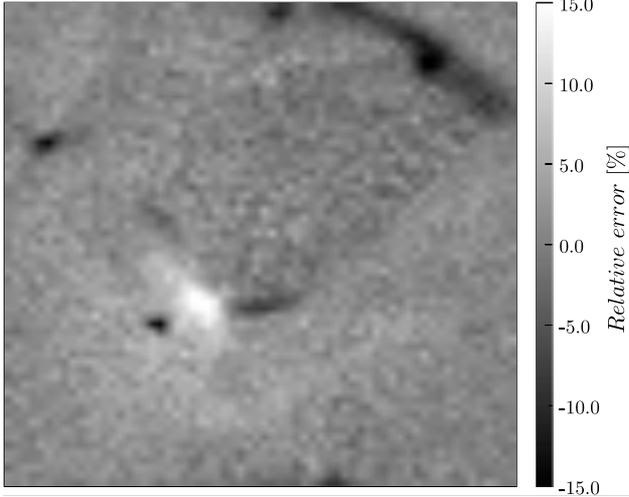
Fig. A.2. Relative errors in the column densities obtained for model C, $\langle A_V \rangle = 1.6^m$, with iterative radiative transfer modelling. The model assumed Gaussian density distribution along the line-of-sight.

the line-of-sight size of the clumps as a further free parameter. Figure A.3b shows results after a simple correction where the column density estimates are increased by the ratio of modelled and true J-band intensities. This is just to illustrate that further improvements are possible.

When optical depth becomes significant, an increase in the column density has gradually less and less effect on the observed intensity. The saturation depends on the wavelength, and changing intensity ratios between different bands carry information on the column density. In the modelling this can be used to break the degeneracy between radiation field and column density. This was tested with the model C and repeating the optimization with the scaling of the external radiation field as free parameters. When observational errors were included, the correct intensity level could still be recovered with accuracy better than 10%. This shows that even if the intensity of the radiation field were not a priori known, the final uncertainty would not be significantly larger than shown in Fig. A.3.

Appendix B: Validity of the basic assumptions

In this section we discuss possible violations of the basic assumptions behind the use of Eq. (1) and examine their effect on the accuracy of the column density estimates.

B.1. Anisotropy of the radiation field

The assumption of a uniform radiation field is violated if (1) the background radiation is anisotropic, (2) the cloud is sufficiently optically thick to cause significant attenuation in its interior, or (3) the cloud contains strong internal radiation sources. The anisotropy of the radiation field was not studied explicitly. However, it is clear that it becomes important only if both conditions (1) and (2) are true. A gradient in the intensity of the incoming radiation causes a corresponding gradient in the column density estimates. In the models the attenuation of the radiation field caused errors only at 10% level between cloud edge and cloud centre. The sky brightness depends on the Galactic coordinates, so that the ISRF is never fully isotropic. The clouds are still illuminated from all sides, and the Galactic plane fills a large solid angle. Therefore, also the difference between cloud edges should
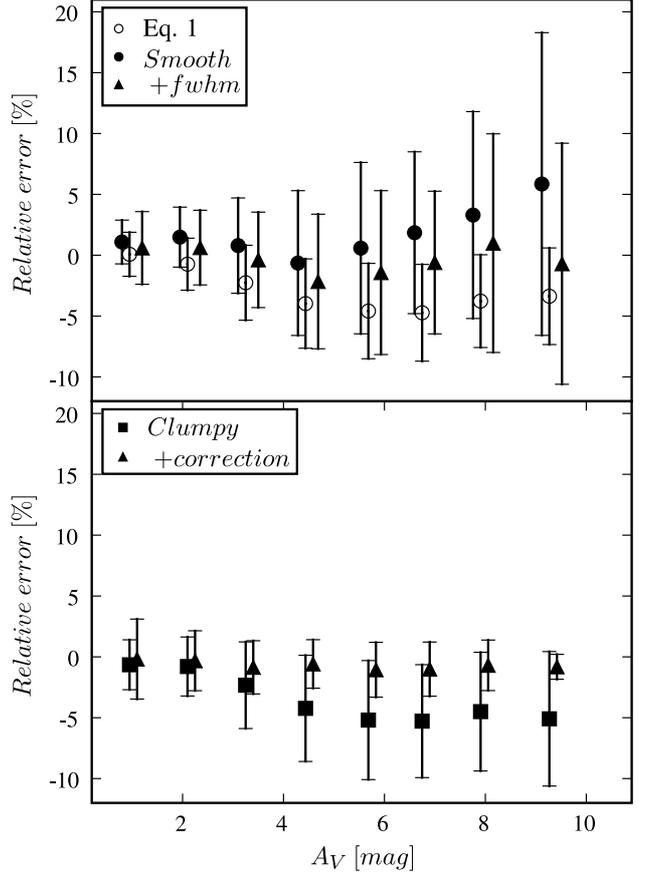

Fig. A.3. Accuracy of column density estimates in the case of model C, $\langle A_V \rangle = 1.6^m$, when three different methods are used. *Upper frame*: original method using Eq. (1) (open circles), iterative modelling with Gaussian line-of-sight density distribution (solid circles), and iterative modelling with Gaussian line-of-sight density distribution with width taken as a free parameter for each sightline (solid triangles). *Lower frame*: results from iterative modelling with clumpy density distribution (squares), and the same after a simple correction based on the error in the predicted J-band intensity (triangles).

exist only at a level below $\sim$10%. Although shadowing by dense regions can cause variations even at relatively small scales, this can still be identified with the help of an extinction map. Once the gradient has been identified or the source of the anisotropy is known, it can be corrected, either by modelling the radiation field or by varying the fit parameters of Eq. (1) as the function of position. Direct re-scaling of the derived column density estimates does not work as well, because of the non-linearity of Eq. (1). In the near-infrared the scattering takes place mostly in the forward direction. This means that the observed surface brightness depends more on the sky brightness behind the cloud than in other directions, and the scaling between surface brightness and column density changes as a function of Galactic coordinates. Of course, this can be corrected by taking into account the true sky brightness distribution available from DIRBE observations. In the first approximation the effect is eliminated if the method is re-calibrated using background stars. There is a small difference between optically thin and optically thick regions, because, in the latter, multiple scattering tends to make the field more isotropic. However, when the surface brightness is used for the column density estimation, radiation can be only moderately optically thick, and the same correction factor should be valid for the whole map.

The radiation field is always attenuated within the cloud. In a homogeneous cloud the gradient is systematic and can be estimated by modelling (e.g., Fig. A.1). In practice the radiation field depends on the unknown 3D cloud structure. Although an exact correction is not possible, our model calculations showed that, by taking into account some general properties of the density field, the accuracy of the column density estimates can be improved (e.g., Fig. A.3). Our results apply to clouds with A_V below 20^m. This limit corresponds to a K-band optical depth of ~1.8. For regions with $\tau_K \gg 1$ the scattered NIR light can not be used as a tracer of the total column density. As the optical depth exceeds unity, the surface brightness saturates and, if the region is sufficiently large, finally decreases towards the column density maximum. The resulting limb-brightening serves only as an indicator of the radius at which the medium becomes optically thick for the observed radiation.

B.2. Internal sources

Internal radiation sources can cause local increase in the surface brightness and decrease the accuracy of the column density estimates in active clouds. If a source is deeply embedded its effect on the surface brightness will be limited to a very small area or it can be readily identified, either directly from surface brightness maps or from a comparison with an extinction map. If the source is outside dense regions, its effect may be more subtle, as was seen in Fig. 16a. A source can illuminate distant filaments while, in projection, nearby regions are apparently unaffected. As an example, we consider the Chamaeleon I cloud where some one hundred embedded sources have been identified (Gómez & Kenyon 2001). The cloud is located at the distance of 160 pc, and on the sky the sources are at mean distance of a few arc minutes from each other. The brightest source has $m_K = 10.2^m$, five sources are brighter than 12^m but most sources are fainter than 13^m. Even the strongest source is fainter than the weakest source in Fig. 16. If this source were located in a dense region, it could be visible in the surface brightness of scattered light, but the effect would be limited to a very small area. Similarly, the contribution of 13^m sources located at one arc minute intervals remains almost two orders of magnitude below the ISRF intensity. If the source is really embedded inside the cloud, the associated elevated NIR dust *emission* should be limited to an even smaller area. Therefore, such embedded sources do not seriously affect the accuracy of the column density estimates.

If cloud contains very strong sources, only in very simple cases can their effect be fully modelled. However, comparison of extinction and surface brightness maps gives a direct way to estimate the effect of internal radiation sources and, at the same time, gives clues about the 3D structure of the object. When the two column density estimates agree, the surface brightness method can be safely used to extend the column density estimation to smaller spatial scales. Close to a source, the surface brightness maps does contain important information about the cloud structure, although weighted according to varying radiation field. In practice, the discrepancies between the two column density estimates can be caused also by problems in the extinction map, for example, if the colour excess data are contaminated by foreground stars or background star cluster or galaxies.

B.3. Dust properties

Dense regions may be problematic, not only because of the attenuation of the radiation field but also because of changes in dust properties. In Sect. 4.2.2 we examined how the results are affected if dust properties do not agree with the model parameters of Eq. (1). Below $A_V \sim 10^m$ the effect was only ~20%. This is almost entirely a systematic effect and does not affect the relative accuracy between regions of different column density. Only above $A_V \sim 10^m$ does the non-linearity of Eq. (1) produce significant A_V-dependence. In this case no attempt was made to correct the values of the erroneous model parameters. In Sect. 4.3 we examined a more realistic case where dust properties changed according to the local density, from $R_V = 3.1$ in low density regions to $R_V = 5.5$ at the highest densities. This time a comparison with low-resolution extinction map was used to re-estimate the parameters of Eq. (1). The result was a well calibrated column density map that had high spatial resolution and was was morphologically very accurate. One set of global parameters was used in Eq. (1). Although this did work reasonably well for both the dense and the diffuse regions, the use of spatially varying parameters might still bring some improvement.

Dust properties affect the ratio between scattered surface brightness and extinction (see Sect. 4.3). When grains become larger the albedo increases and scatterings are oriented more in the forward direction. This affects the transport of radiation during the first phase (see Sect. 2 and Fig. 1) and, for a given extinction, makes the field more uniform within the cloud. For clouds with $A_V \sim 10^m$ the variations on the plane of the sky are small, and changes in the albedo and scattering function can only have a minor effect. The main effect comes from the fact that the observed surface brightness is directly scaled by the albedo at the position of the last scattering. During the second phase the radiative transfer equation is similar as for the extinction of the background stars and depends on the extinction cross section. The net effect is that the albedo acts as a multiplicative factor that scales the surface brightness relative to the extinction. Conversely, the ratio of surface brightness and extinction could be used to trace variations in the average grain size. However, as shown by Fig. 15, the effect may be small and its detection and separation from all the other possible effects is not straightforward.

B.4. Other sources contributing to the NIR surface brightness

We have assumed that the observed surface brightness is due to dust scattering inside the cloud. If there are other significant sources, their contribution must be determined and removed or the column density estimates are correspondingly in error. We discuss three potential factors affecting the NIR surface brightness: Thermal dust emission, emission lines, and the role of the NIR background.

B.4.1. Thermal dust emission

At optical wavelengths scattering dominates over the thermal emission from cold dust particles. In the mid-infrared the situation is already reversed and emission from transiently heated small particles and large molecules is the dominant component. In the mid-infrared the strong emission bands are generally attributed to PAH molecules. However, there is also a broad continuum that extends to the NIR, although significantly diminished. We estimate the thermal dust emission based on the model of Li & Draine (2001). According to their Fig. 8, the expected dust emission in the K band is $\lambda I_\lambda \sim 2 \times 10^{-27}$ erg/s/sr/H. Excluding all absorption, the expected intensity for dust column with $A_V = 1.6$ is ~4.5×10^{-20} erg/s/cm²/sr/Hz. For

similar A_V the surface brightness of scattered radiation was in our calculations $\sim 2 \times 10^{-19}$ erg/s/cm²/sr/Hz, the number including some reduction caused by absorption. Therefore, in an optically thin case the emission could contribute some 20% to the total surface brightness. However, while the scattering involves here only one NIR wavelength, dust emission depends on the heating that takes place through shorter wavelengths. This is especially true for the NIR emission that requires grain temperatures of the order of 1000 K and, consequently, heating by energetic photons. At $A_V = 1^m$ the attenuation is in the U-band a factor of ~ 5 and even the V-band close to a factor of three. Therefore, dust emission is restricted to cloud surfaces, and, even in translucent clouds, its contribution to the total surface brightness is only a few per cents. In more optically thick clouds the ratio between scattered and emitted intensity increases, until also the scattered K-band intensity saturates after $A_V \sim 10^m$. In the H-band the expected dust emission is only half of the value in the K-band. Moreover, there is evidence that the abundance of small grains decreases rapidly in dense clouds (e.g., Stepnik et al. 2003), further reducing the relative amount of NIR emission expected from optically thick clouds.

Compared with the continuum, the contribution of possible PAH lines and other features is small (e.g., Gordon et al. 2000; Mattioda et al. 2005b). In the Li & Draine model small graphite grains are responsible for most of the NIR continuum. For *ionized* PAHs the NIR absorption cross sections may be significantly higher than assumed by that model (see Mattioda et al. 2005a,b). This may affect the interpretation of the source of near-infrared continuum but, because the modelled small grain contribution was well above the PAH continuum, the effect on total predicted emission would be much smaller. Furthermore, within most of the volume of our clouds the radiation field is both softer and weaker than the normal ISRF, thus reducing the degree of PAH ionization. On the other hand, Sellgren et al. (1996 and references therein) observed in several optical reflection nebulae significant NIR dust emission that was similarly attributed to either very small, transiently heated dust grains or PAH-type molecules. In the K band the emission exceeded the predicted scattering when the temperature of the central star was larger than ~ 6000 K. One can make a conservative assumption that the ratio of the emitted and scattered radiation follows the ratio of incoming K-band and V-band intensities. For a 6000 K black body this ratio is 1.66, while in the case of the ISRF (Mathis et al. 1983) the ratio is only 0.42, i.e., lower by a factor of four. In reality the reduction can be much larger, because the heating is likely to require large flux of UV-photons, because of the strong attenuation of the optical-UV field in optically thick clouds, and because the observed NIR emission may be related to a difference in dust properties. Therefore, the results of Sellgren et al. are not in contradiction with our assumption that in a cloud illuminated by normal ISRF the scattering stands for most of the observed surface brightness.

Further evidence for NIR dust emission comes from DIRBE observations. Bernard et al. (1994) presented a spectrum for the average cold diffuse medium at $|b| = 5$ deg. After subtraction of zodiacal light and stellar emission, the remaining signal was 0.023 MJy/sr at 3.5 μm and 6.7 MJy/sr at 100 μm, corresponding to $A_V \sim 0.5$. Only a minor fraction of the 3.5 μm signal can be due to scattered light. If one assumes that the 3.5 μm value is caused entirely by emission and further assumes a flat spectrum, $\nu I_\nu = $ constant, the predicted K-band emission would be 1.5×10^{-19} erg/s/cm²/sr/Hz. For this low A_V the value is higher than the expected intensity of the scattered light, while in the J-band the emission would drop to $\sim 10\%$ of the scattered

intensity. Arendt et al. (1998) correlated different DIRBE bands against the 100 μm band at $|b| < 30$ deg. The correlation coefficient between 3.5 μm and 100 μm intensities was, 1.8×10^{-3}, i.e., lower by almost a factor of two. The values might still be overestimated, if the DIRBE values contained additional signal from incompletely removed stars or from scattering, or were significantly affected by the presence of the 3.3 μm PAH feature.

Flagey et al. (2006) have recently studied NIR emission using ISO and Spitzer data and modelled emission seen at diffuse sightlines. Based on their model the extrapolated value at 2 μm is ~ 0.03 MJy sr^{-1} for $N_H = 10^{21}$ cm^{-2} (see their Fig. 9). At $A_V = 0.5^m$ this would correspond to 1.9×10^{-19} erg/s/cm^{-2}/sr/Hz, i.e., a slightly higher intensity than the previous Bernard et al. (1994) value. The NIR continuum was modelled with a 1100 K gray body which is typical of reflection nebulae. A lower colour temperature of the continuum would very rapidly reduce the predicted K-band intensity. The model of Flagey et al. 2006 applied to diffuse medium in the inner Galaxy where, according to their own estimate, the radiation field has intensity three times the local ISRF. The emission should be correspondingly smaller in local clouds. A critical question is, at what A_V the UV-field has attenuated so much that the scattering dominates also the K-band surface brightness.

The NIR dust emission remains uncertain because of the lack of observations and because of the significant uncertainties in the modelled NIR emission (see also Zubko et al. 2004). There is observational evidence that at higher column densities the NIR surface brightness is clearly dominated by scattering (e.g., Lehtinen & Mattila 1996; Foster & Goodman 2006). The DIRBE results are consistent with those observations, if the dust emission comes mainly from diffuse material. In dense clouds, the emission would be restricted to a narrow surface layer and it would be distributed rather evenly over the whole cloud. Part of the signal may be removed in on-off observations, and the remainder would not be strongly correlated with the column density. Furthermore, if the parameters of Eq. (1) are determined from observations, e.g., from comparison with extinction data, the contribution of dust emission is already taken into account. The functional form of Eq. (1) can accommodate some contribution from emission. If emission is strong, an additional offset term is required. If the K-band turns out to contain significant emission, its use can be restricted to opaque regions, where dust emission is low. Indeed, the K-band data is essential only in very dense regions, where the shorter wavelength data suffer from significant saturation. Furthermore, the K-band observations are relatively more time-consuming, and at low column densities the S/N-ratio tends to be worse than for the other bands. Conversely, deep NIR observations will enable mapping of the relative intensity of the dust emission and scattering.

B.4.2. Emission lines

The NIR bands can contain line emission from smaller molecules and ions. In cold clouds the excitation is far too low to produce strong NIR lines, e.g., from CO and H_2 molecules. Significant line emission can occur either in photon dominated regions (PDRs) on the cloud surface or in shocks triggered, for example, by the outflows from young stellar objects (YSOs) within the cloud. The presence of strong PDR regions would also contradict the assumption of an isotropic background. Foster & Goodman 2006 discussed the possible contribution of H_2 lines based on the models of Black & Dishoeck (1987). They noted that the observed J- and H-band intensities showed no indication of line emission. Indeed, in the models of Black & Dishoeck,

assuming a cloud illuminated with normal ISRF, the effect of H_2 should remain insignificant.

YSOs are commonly associated with molecular outflows that are driven by fast jets. Along its path the jets cause shocks, Herbig-Haro objects, that are visible in the NIR, especially through many H_2 lines. The strongest line, the H_2 1–0 $S(1)$ line at 2.12 μm, falls within the K-band filter. The J and H bands have similarly some contribution from, e.g., the excited [FeII] lines at 1.24 and 1.64 μm (Reipurth 1999). Therefore, along the jet all NIR bands may be contaminated by line emission. However, if Herbig-Haro objects are observed, they are usually clearly aligned along the jets, which must be masked out from subsequent analysis. If no outflow is detected, for example, if even the brightest knots fall below the detection limit, the jet will clearly have no effects on the column density estimates. At the end of the outflow then bowshocks may also cause enhanced NIR surface brightness. Bowshocks can be much larger than the Herbig-Haro regions, and may be located very far from the driving source and the visible part of the jet. The shape of a bowshock depends on the density structure of the ambient material that is interacting with outflow. Therefore, a purely morphological identification of bowshocks may be difficult. Strong bowshocks can be recognized based on anomalous intensity ratios, while faint ones may go unnoticed and cause some errors in the column density estimates.

B.4.3. Background radiation

In on-off measurements one measures the difference between the signal from the source and the background. If the intensity of the diffuse background, $S_{\rm bg}$ is large behind the source without significantly affecting the total amount of radiation entering the cloud, the observed signal will decrease by an amount of $S_{\rm bg}(1 - e^{-\tau})$, where τ is the optical depth of extinction for a sightline through the cloud. As long as this term is smaller than the surface brightness due to scattering, the dependence between column density and surface brightness will only become more shallow. As an empirical description of this dependence Eq. (1) should remain approximately valid, provided that the parameters of the equation take the background into account. Re-calibration using the colour excess data would automatically accomplish this. If $S_{\rm bg}$ is equal to the surface brightness of scattered light, column densities could no longer be estimated, because the observed signal would be zero. If $S_{\rm bg}$ is larger and sufficiently constant, the cloud structure could, of course, be traced by the absorption.

We will first consider the cosmological IR background (CIRB), $S_{\rm CIRB}$. If the absorption due to the Galaxy is ignored, this is an isotropic component. If one considers optically thin clouds or a perfectly spherical cloud, the *scattered* CIRB photons have no effect on the observed surface brightness: The distribution of outcoming photons is also isotropic. If the cloud is optically thick and inhomogeneous, the radiation field is no longer isotropic inside the cloud. Therefore, the amount of radiation scattered away from one line-of-sight is no longer equal to the amount of radiation scattered from other directions into that direction. However, this imbalance is only a small fraction of the scattered CIRB intensity and this variation in the surface brightness of the scattered CIRB photons can be safely ignored. Because of the *absorbed* radiation the observed intensity decreases by $S_{\rm bg}(1 - e^{-\tau})$, the term τ being the optical depth for absorption. In the optically thin case the scattering can be ignored altogether, because each scattered photons escapes the cloud and the surface brightness of the cloud is identical with
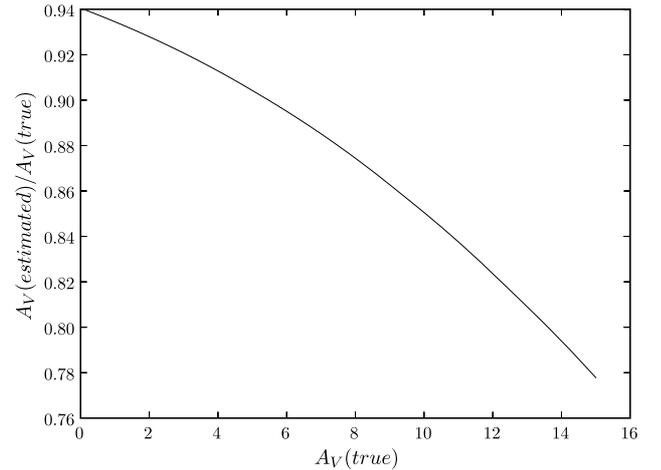

Fig. B.1. Ratio of column density estimates and true column density when the analysis ignores an existing background surface brightness. In the plot the column densities are derived based on K-band data and using the average parameters obtained from the numerical models. The background intensity is 1.64×10^{-19} erg/s/cm^2/Hz/sr (see text).

the background sky. The depression in the surface brightness of optically thicker clouds has been calculated by Mattila (1976, Table A2). When the optical depth is below 4 and the contribution from scattering is ignored, the relative error in our estimate of the change in the surface brightness is less than ~15%. This is sufficient accuracy for our purposes.

The tentative K-band CIRB detection of Gorjian et al. (2000) was $S_{\rm bg} = 1.64 \times 10^{-19}$ erg/s/cm^2/Hz/sr. This high value corresponds almost to the mean surface brightness of scattered radiation in our $\langle A_{\rm V} \rangle = 1.6^{\rm m}$ models. In on-off observations the addition of this background would decrease the measured K-band surface brightness excess roughly by $S_{\rm bg}(1 - e^{-0.049 \times A_{\rm V}})$, the factor 0.049 being the ratio of K-band absorption and $A_{\rm V}$. The decreased surface brightness leads to an underestimation of the column densities. The magnitude of this effect is shown in Fig. B.1, assuming that the parameters of Eq. (1) are determined *without* taking the background into account and only K-band data are used. If the background level were known or the parameters were corrected using the extinction data, the error could be almost completely removed. Therefore, in practice it has little effect on the accuracy of the column density estimates. The CIRB intensity used above is very uncertain, and the true value may turn out to be significantly lower (e.g., Dwek et al. 2005; Aharonian et al. 2006). On the other hand, the effect of the CIRB is relatively higher in the J- and H-bands, because of the higher optical depth and possibly higher CIRB intensity (Hauser & Dwek 2001).

In the modelling we have assumed that the cloud is illuminated by the normal ISRF. The diffuse background was not included in the calculated surface brightness nor was a background subtraction included in the subsequent analysis. If the ISRF is caused by discrete point sources, no background subtraction is necessary, because the surface brightness can be determined on the empty sky between sources. However, if the ISRF contains a significant diffuse component, the observed values will again be reduced by $S_{\rm bg}^{\rm diffuse}(1 - e^{-\tau})$, τ being the optical depth for absorption, and qualitatively the effect is the same as in Fig. B.1. If the background intensity is approximately isotropic, the main effect comes from absorption, and the scattering can again be ignored. Diffuse background could consist of unresolved stars or of photons that are scattered

from background clouds. In the latter case the mapping of the foreground cloud may be impossible, because its contribution to the observed surface brightness cannot be separated from the background. The effect of faint stars depends on the direction on the sky and the resolution and sensitivity of the observations. A crude estimate can be made assuming a slope of 0.35 in the (mag, $\log_{10} N$)-relation (see Sect. 4.3). The relation is shallow enough that, in the total intensity, the contribution of a magnitude bin decreases with increasing magnitude. For observations discussed in Sect. 4.2 the limiting K-band magnitude is far fainter than 20^{m}. If one assumes that the contribution of stars brighter than 20^{m} can be separated from the diffuse background and stars are integrated down to 40^{m}, the contribution of the unresolved stars remains below 10% of the total surface brightness. The net effect on the column density estimates is again some fraction of this. For a given direction on the sky, more accurate estimates and possible correction can be made using Galactic models of stellar distribution (e.g., Cohen 1994). However, our estimate is rather conservative, and, in most cases, the effect of unresolved stars can be ignored. The Galactic plane may be an important exception, because of the anisotropy of the radiation field, and the source confusion which makes the separation of the diffuse background difficult.

In the NIR the zodiacal light is by far the strongest diffuse component but, because it has a smooth spatial distribution and it resides between the observer and the studied cloud, it has little effect on the column density estimation. Some problems can still be caused by surface brightness gradients across large maps close to the ecliptic plane, or, in rare cases, comet trails that introduce small scale structure in the surface brightness (e.g., Kelsall et al. 1998; Nakamura et al. 2000).